Optimal surface-tension isotropy in the Rothman-Keller color-gradient lattice Boltzmann method for multiphase flow

Peter Mora[*]
College of Petroleum Engineering and Geosciences, King Fahd University of Petroleum and Minerals, Dhahran 31261, Saudi Arabia

Gabriele Morra[†]
Department of Physics and School of Geosciences, University of Louisiana at Lafayette, Lafayette, Louisiana 70503, USA

David A. Yuen[‡]
Department of Applied Physics and Applied Mathematics, Columbia University, New York, New York 10027, USA and Department of Information Science and Engineering and College of Marine Geosciences, Ocean University of China, Qingdao 266100, China

(Received 8 July 2020; revised 2 November 2020; accepted 11 January 2021; published 3 March 2021)

The Rothman-Keller color-gradient (CG) lattice Boltzmann method is a popular method to simulate two-phase flow because of its ability to deal with fluids with large viscosity contrasts and a wide range of interfacial tensions. Two fluids are labeled red and blue, and the gradient in the color difference is used to compute the effect of interfacial tension. It is well known that finite-difference errors in the color-gradient calculation lead to anisotropy of interfacial tension and errors such as spurious currents. Here, we investigate the accuracy of the CG calculation for interfaces between fluids with several radii of curvature and find that the standard CG calculations lead to significant inaccuracy. Specifically, we observe significant anisotropy of the color gradient of order 7% for high curvature of an interface such as when a pinchout occurs. We derive a second order accurate color gradient and find that the diagonal nearest neighbors can be weighted differently than in the usual color-gradient calculation such that anisotropy is minimized to a fraction of a percent. The optimal weights that minimize anisotropy for the smallest radius of curvature interface are found to be $w = (0.298, 0.284, 0.275)$ for diagonal nearest neighbors for the cases of the interface smoothing parameter $\beta = (0.5, 0.7, 0.99)$, somewhat higher than the $w = 0.25$ value derived by Leclaire *et al.* [Leclaire, Reggio, and Trepanier, Computers and Fluids **48**, 98 (2011)] based on obtaining isotropic errors to second order. We find that use of these optimal w values yields over a factor of 10 decrease in anisotropy and over a factor of 30 decrease in mean anisotropy relative to using the standard $w = 1$ value. And we find a factor of about 2 decrease in the anisotropic error and up to factor 15 decrease in mean anisotropic error relative to the choice of $w = 0.25$ for small radius of curvature interfaces. The improved CG calculations will allow the method to be more reliably applied to studies of phenomenology and pore scale processes such as viscous and capillary fingering, and droplet formation where surface-tension isotropy of narrow fingers and small droplets plays a crucial role in correctly capturing phenomenology. We present an example illustrating how different phenomena can be captured using the improved color-gradient method. Namely, we present simulations of a wetting fluid invading a fluid filled pipe where the viscosity ratio of fluids is unity in which droplets form at the transition to fingering using the improved CG calculations that are not captured using the standard CG calculations. We present an explanation of why this is so which relates to anisotropy of the surface tension, which inhibits the pinchouts needed to form droplets.

DOI: 10.1103/PhysRevE.103.033302

I. INTRODUCTION

The lattice Boltzmann method (LBM) allows fluid dynamics to be modeled by simulating the movement and collision of particle distributions on a discrete lattice in two or three dimensions. Lattice Boltzmann methods have their origins in lattice gas automata (LGA) in which particles move and collide on a discrete lattice representing a simplified discrete version of molecules moving and colliding in a gas. LGA were first proven by Frisch *et al.* [1] to yield the Navier-Stokes equations in the macroscopic limit. These initial LGA models were unconditionally stable and conserved mass and momentum perfectly. However, they were computationally expensive with averaging needed over space to obtain the macroscopic equations and, furthermore, costly calculations were required to calculate the collision term. Since the initial LGA models, the method has been extended to model distributions of particles moving and colliding on a lattice. In these lattice Boltzmann methods, one is solving the classical Boltzmann equation on a discrete lattice. Since an efficient method via relaxation was developed to calculate the collision term due

[*]wolop2008@gmail.com
[†]morra@louisiana.edu
[‡]daveyuen@gmail.com

to Bhatnagar, Gross, and Krook [2] (the BGK method [3,4]), research and applications of the lattice Boltzmann method have undergone an explosion [5–8]. Numerous studies have been conducted of thermal convection [9–15], and a large number of multiphase LBMs have been developed including the Shan and Chen multicomponent multiphase LBM [16], the Rothman and Keller (RK) color-gradient multiphase LBM [17], free-energy based multiphase LBMs [18]), Inamuro's multiphase LBM [19], and the He-Chen-Zhang multiphase LBM [9]). Multiphase LBMs remain a highly active research field (see Huang *et al.* [5] for a summary of the main multiphase LBMs and their application).

The RK color-gradient multiphase LBM has the advantage over the other most widely used two-phase LBM—the Shan and Chen LBM [16]—that it allows much higher viscosity ratios to be simulated ranging from 0.01 to 100 using the single relaxation time BGK method, and at least 0.002 to 500 using the more stable multiple relaxation time LBM [20]. And provided the color gradient is computed with a more isotropic high order color-gradient operator [21], the RK LBM can also simulate high density ratios up to $O(10^3)$. The RK color-gradient multiphase LBM has successfully been applied to simulate viscous fingering, capillary fingering, and stable displacement behavior [22], and has been applied to the study of imbibition and drainage of porous media in three dimensions [23]. In the following, we study the accuracy of the RK LBM and, in particular, the anisotropic error of the color-gradient calculations.

One issue with the RK color-gradient method is that the numerical error in the color-gradient calculations leads to anisotropy of the interfacial tension and, consequently, spurious currents [6,7] and potentially erroneous results, especially when the interface has a small radius of curvature and, hence, the highest error. This can be mitigated by use of high order finite-difference calculations to compute the color gradient such as developed by Leclaire *et al.* [21,24] and applied by Leclaire *et al.* [23] to study imbibition and drainage in three-dimensional porous media. In this approach, a fourth or higher order distributed finite-difference operator is applied in fluid sites where the operator was developed to achieve isotropy of the color-gradient error to a given order. On sites adjacent to walls, a standard forward, centered, or backward discrete gradient operator is used [25]. A disadvantage of this approach is its increased computational cost with both more calculations and communications required to compute the gradient. A second disadvantage is that it is only accurate to higher than second order in the fluid sites that are not adjacent to walls where the CG calculations are accurate only to first or second order.

An alternative approach to this high order finite-difference based method is to remain accurate to second order and, hence, to use only the nearest neighbors, and to change the weights in the gradient calculation as developed by Leclaire *et al.* [21]. This method leads to isotropy of the error in the color-gradient calculations up to second order in space using a weight of diagonal nearest neighbors of $w = 0.25$ relative to nearest neighbors along the Cartesian axes. With their approach, Leclaire *et al.* also reduced spurious currents by an order of magnitude and, for higher order schemes only, removed the limitation of the standard RK model to handle high density ratios up to $O(10^3)$.

In the following, we adopt the basic idea of remaining second order accurate and changing the weights in the color-gradient calculation to minimize anisotropy. Staying second order accurate means that the color-gradient calculation is local which is desirable for pore scale modeling in complex porous media, an important area of research. We present the general formula for a second order accurate color-gradient calculation which allows any weight to be placed on the diagonal nearest neighbors in the color-gradient calculation relative to the Cartesian nearest neighbors. Rather than adopting the relative weight derived by Leclaire *et al.* of $w = 0.25$ for diagonals which obtains isotropic errors to second order, we study the numerical error in the color gradient of three droplets with different radii of curvature over the complete range of relative weights. The benefit of focusing on the actual error for specific droplet radii of curvature is that it allows one to gain a more detailed understanding of the anisotropic error in the color gradient, and to minimize anisotropic error of the color gradient for small radius of curvature droplets in the LBM, which have the greatest effect on transitions such as droplet formation.

II. NUMERICAL SIMULATION METHODOLOGY

In this paper, we apply the RK multiphase lattice Boltzmann model which was originally derived for a lattice gas automaton [26], and later extended to the LBM by Guntensen *et al.* [27] and Latva-Kokko and Rothman [17]. The color-gradient RK lattice Boltzmann model involves modeling particle distributions denoted f_α^k of two fluids (red and blue for $k = 1$ and 2) moving and colliding on a discrete lattice. The total number density of the two phase fluid is given by

$$f_\alpha(\mathbf{x}, t) = \sum_k f_\alpha^k(\mathbf{x}, t),$$

where the subscript α specifies the direction in the lattice, and the superscript $k = 1, 2$ denotes fluid 1 and fluid 2.

There are three steps in this method, which are (i) streaming, (ii) collision, and (iii) "recoloring." The streaming step is the same as the standard lattice Boltzmann method streaming step. Namely, in one time step, the particle distributions can move by one lattice spacing along the orthogonal axes, or along diagonals. We use the standard LBM notation $DnQm$ for a simulation in $D = n$ dimensions, and with $Q = m$ velocities on the discrete lattice. In the following, we restrict ourselves to two dimensions and use the $D2Q9$ lattice Boltzmann lattice arrangement shown in Fig. 1. In this lattice, we define $f_\alpha^k(\mathbf{x}, t)$ as the number density of particles of fluid k moving in the α direction where the $Q = 9$ velocities are given by

$$\mathbf{c}_\alpha = [(0, 0), (1, 0), (-1, 0), (0, 1), (0, -1), (1, 1), (-1, -1), (1, -1), (-1, 1)]\Delta x/\Delta t.$$

This choice means that $\mathbf{c}_0$ is the zero velocity vector and therefore represents stationary particles, and $\mathbf{c}_\alpha = -\mathbf{c}_{\alpha+1}$ for $\alpha = (1, 3, 5, 7)$ are the velocities in the eight directions shown in Fig. 1. The lattice is unitary so the lattice spacing and time step are $\Delta x = \Delta t = 1$. The streaming step is specified as

$$f_\alpha^k(\mathbf{x} + \mathbf{c}_\alpha \Delta t, t + \Delta t) = f_\alpha^k(\mathbf{x}, t). \quad (1)$$

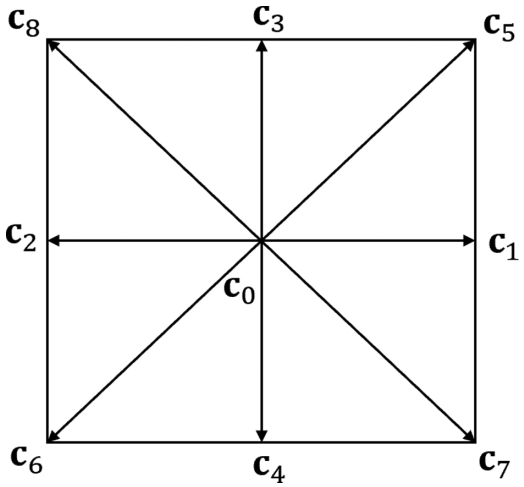

FIG. 1. The $D2Q9$ lattice.

The collision step for the two-phase LBM involves two terms and can be written as [17]

$$f_\alpha^{k*}(\mathbf{x},t) = f^k(\mathbf{x},t) + \left(\Delta f_\alpha^k\right)^1 + \left(\Delta f_\alpha^k\right)^2, \tag{2}$$

where the asterisk superscript denotes the postcollision distributions, and $(\Delta f_\alpha^k)^1$ and $(\Delta f_\alpha^k)^2$ are the two collision terms which represent how the particle distributions change during each time step due to collision $[(\Delta f_\alpha^k)^1]$ while encouraging color segregation $[(\Delta f_\alpha^k)^2]$. The first collision term is nearly the same as the standard collision term of the LBM and is given by

$$\left(\Delta f_\alpha^k\right)^1 = \frac{1}{\tau}\left[f_\alpha^{k,\mathrm{eq}}(\mathbf{x},t) - f_\alpha^k(\mathbf{x},t)\right] \tag{3}$$

where τ is the relaxation time and $f_\alpha^{k,\mathrm{eq}}(\mathbf{x},t)$ is the equilibrium distribution which is given by

$$\begin{aligned} f_\alpha^{k,\mathrm{eq}} &= \rho_k\left(C_\alpha^k + w_\alpha\left[\frac{\mathbf{c}_\alpha\cdot\mathbf{u}}{c_s^2} + \frac{(\mathbf{c}_\alpha\cdot\mathbf{u})^2}{2c_s^4} - \frac{\mathbf{u}^2}{2c_s^2}\right]\right) \\ &= \rho_k\left(C_\alpha^k + w_\alpha\left[3(\mathbf{c}_\alpha\cdot\mathbf{u}) + \frac{9}{2}(\mathbf{c}_\alpha\cdot\mathbf{u})^2 - \frac{3}{2}\mathbf{u}^2\right]\right) \end{aligned} \tag{4}$$

where $c_s = \Delta x/(\sqrt{3}\Delta t) = 1/\sqrt{3}$ is the speed of sound in the lattice. The above equilibrium distribution is the same as the standard equilibrium distribution except for the rest factor C_α instead of w_α. The coefficients C_α are given by [28]

$$C_\alpha = \begin{cases} \alpha_k & \alpha = 0 \\ \frac{1-\alpha_k}{5} & \alpha = 1,2,3,4, \\ \frac{1-\alpha_k}{20} & \alpha = 5,6,7,8 \end{cases} \tag{5}$$

where α_k is a parameter that enables the density of the two fluids to be adjusted [28,29] and is given by

$$\frac{\rho_1}{\rho_2} = \frac{1-\alpha_2}{1-\alpha_1}. \tag{6}$$

The other weights are the same as the standard LBM. Namely, $w_0 = 4/9$, $w_\alpha = 1/9$ for $\alpha = 1,2,3,4$ and $w_\alpha = 1/36$ for $\alpha = 5,6,7,8$. The macroscopic density of the two fluids is given by

$$\rho_k = \sum_\alpha f_\alpha^k, \tag{7}$$

the total density of the fluid is given by

$$\rho = \sum_k \rho_k, \tag{8}$$

and the momentum of the fluid is given by

$$\rho\mathbf{u} = \sum_k\sum_\alpha f_\alpha^k\mathbf{c}_\alpha. \tag{9}$$

The relaxation time τ_k relates to the kinematic viscosity ν_k of each fluid as follows:

$$\nu_k = c_s^2(\tau_k - 0.5)\Delta t. \tag{10}$$

At the interface between fluids, the relaxation time changes abruptly, which cannot be handled well numerically. Therefore, in order for the relaxation parameter to change smoothly at the interface, it is interpolated as follows [28]:

$$\tau(\mathbf{x}) = \begin{cases} \tau_1 & \psi > \delta \\ g_1(\psi) & 0 < \psi \leqslant \delta \\ g_2(\psi) & -\delta \leqslant \psi \leqslant 0 \\ \tau_2 & \psi < -\delta \end{cases}, \tag{11}$$

where ψ is given by

$$\psi(\mathbf{x}) = \frac{\rho_1(\mathbf{x}) - \rho_2(\mathbf{x})}{\rho_1(\mathbf{x}) + \rho_2(\mathbf{x})}, \tag{12}$$

and $g_1(\psi) = s_1 + s_2\psi + s_3\psi^2$, $g_2(\psi) = t_1 + t_2\psi + t_3\psi^2$, $s_1 = t_1 = 2\tau_1\tau_2/(\tau_1+\tau_2)$, $s_2 = 2(\tau_1 - s_1)/\delta$, $s_3 = -s_2/(2\delta)$, $t_2 = 2(t_1 - \tau_2)/\delta$, and $t_3 = t_2/(2\delta)$. In these equations, the positive free parameter δ affects interface thickness and is usually set as $\delta = 0.98$.

The second collision term is more complex and there are several forms in the literature. Here, we use the term as written in Reis and Phillips [29]:

$$\left(\Delta f_\alpha^k\right)^2 = A|\mathbf{F}|\{w_\alpha[\cos(\lambda_\alpha)|\mathbf{c}_\alpha|]^2 - B_\alpha\}, \tag{13}$$

where $\mathbf{F}(\mathbf{x},t)$ is the color gradient calculated by Latva-Kokko and Rothman [17],

$$\mathbf{F}(\mathbf{x},t) = \sum_\alpha \mathbf{c}_\alpha[\rho_1(\mathbf{x}+\mathbf{c}_\alpha\Delta t,t) - \rho_2(\mathbf{x}+\mathbf{c}_\alpha\Delta t,t)], \tag{14}$$

λ_α is the angle between $\mathbf{F}(\mathbf{x},t)$ and $\mathbf{c}_\alpha$, and A is a parameter that controls interfacial tension. In the above equation, the cosine term is given by

$$\cos(\lambda_\alpha) = \frac{\mathbf{c}_\alpha\cdot\mathbf{F}}{|\mathbf{c}_\alpha||\mathbf{F}|}, \tag{15}$$

and $B_0 = -4/27$, $B_\alpha = 2/27$ for $\alpha = 1,2,3,4$ and $B_\alpha = 5/108$ for $\alpha = 5,6,7,8$. Reis and Phillips [29] have shown that the above parameters yield the correct term for interfacial tension σ in the Navier-Stokes equations, and Huang *et al.* [22] have shown that the interfacial tension σ is approximately proportional to A.

The final step in the lattice Boltzmann method for two phase flow is a so-called recoloring step, which achieves separation of the two fluids. This is achieved as follows [17]:

$$f_\alpha^1 = \frac{\rho_1}{\rho} f_\alpha^* + \beta \frac{\rho_1 \rho_2}{\rho^2} f_\alpha^{\rm eq}(\rho, \mathbf{u} = 0) \cos(\lambda_\alpha), \tag{16}$$

and

$$f_\alpha^2 = \frac{\rho_2}{\rho} f_\alpha^* - \beta \frac{\rho_1 \rho_2}{\rho^2} f_\alpha^{\rm eq}(\rho, \mathbf{u} = 0) \cos(\lambda_\alpha), \tag{17}$$

where $f_\alpha^* = \sum_k f_\alpha^{k*}$, and A and $\beta \in (0, 1]$ are adjustable parameters that affect the interfacial properties. Namely, β affects the interfacial thickness, and A and τ_1 and τ_2 affect the interfacial tension. In the above recoloring equation, the equilibrium distribution at zero velocity is given by the standard equilibrium distribution, namely,

$$f_\alpha^{\rm eq}(\rho, \mathbf{u} = 0) = w_\alpha \rho.$$

The pressure in the flow field is obtained from the equation of state and can be calculated as

$$p = c_s^2 \rho.$$

In the lattice Boltzmann method, one achieves no-slip boundary conditions by "bounce-back" boundary conditions at the solid interface. Namely, particle number densities bounce back in the direction they came from at fluid-solid interfaces. The RK model for two phase flow allows any wetting contact angle θ_w to be specified by setting the densities of the two fluids in the solid region [17] through

$$\theta_w = \cos^{-1}\left(\frac{\rho_{w1} - \rho_{w2}}{\rho_i}\right), \tag{18}$$

where ρ_{w1} is the density of fluid 1 in the solid regions, ρ_{w2} is the density of fluid 2 in the solid regions, and ρ_i is the initial density of the majority component $=\rho_2$. Namely, we set

$$\rho_{w1} = \rho_i \frac{1 + \cos(\theta_w)}{2}, \tag{19}$$

and

$$\rho_{w2} = \rho_i \frac{1 - \cos(\theta_w)}{2}. \tag{20}$$

III. COLOR-GRADIENT CALCULATIONS

The standard color-gradient calculations for $\mathbf{F}(\mathbf{x}, t)$ specified by Latva-Kokko and Rothman [17] are given by Eq. (14) and repeated here:

$$\mathbf{F}(\mathbf{x}, t) = \sum_\alpha \mathbf{c}_\alpha [\rho_1(\mathbf{x} + \mathbf{c}_\alpha \Delta t, t) - \rho_2(\mathbf{x} + \mathbf{c}_\alpha \Delta t, t)]$$
$$= \sum_\alpha \mathbf{c}_\alpha D(\mathbf{x} + \mathbf{c}_\alpha \Delta t, t). \tag{21}$$

Hence, the color gradient is computed using the color difference $D = \rho_1 - \rho_2$ at the eight surrounding nodes from the lattice site. In the following, we make use of Taylor's expansions to derive a general formula for the color-gradient calculations that is accurate to second order.

Taylor series based calculation of the color gradient

Taylor's series are widely used to calculate finite-difference derivatives of variables for numerical solutions to partial differential equations. In this method, a derivative is approximated as the sum of the function at adjacent points multiplied by a set of coefficients, and the coefficients are obtained by solving algebraic equations such that the approximation converges to the derivative to a given order in Δx. For example, $\partial f/\partial x \approx c_1 f(x + \Delta x) + c_2 f(x - \Delta x) = [f(x + \Delta x) - f(x - \Delta x)]/(2\Delta x)$, i.e., $c_1 = 1/(2\Delta x) = -c_2$, is a typical centered finite difference which converges at a rate of $O(\Delta x^2)$. In the following, we derive the finite-difference formula for the color-gradient calculation using a weighted sum of the function at adjacent points. In the following, we denote the color difference as $D = \rho_1 - \rho_2$, and follow the standard finite-difference approach to calculate the finite-difference approximation. Specifically, if we wish to derive the finite-difference approximation for a derivative using only the values of the function at the nearest neighbors of a given lattice site, we can write

$$\frac{\partial D}{\partial x} \approx \sum_\alpha c_\alpha D(\mathbf{x} + \Delta \mathbf{x}_\alpha), \tag{22}$$

where $\Delta \mathbf{x}_\alpha = \mathbf{c}_\alpha \Delta t$ is the vector pointing to the adjacent lattice site in the α direction. It is important to note that in the above, we use boldface $\mathbf{c}_\alpha$ to denote the particle velocity in the α direction, whereas italic c_α represents the scalar coefficients of the finite-difference formula. In Eq. (22), which is applicable for the two-dimensional (2D) LBM, we are computing a weighted sum of the values of the color difference D at the eight adjacent lattice sites in the orthogonal and diagonal directions. Note that we include in the sum $\alpha = 0$ for completeness, although as we will see, the value of D at the central point plays no role (i.e., we will find that $c_0 = 0$).

Expanding the values of D as Taylor's series about $\mathbf{x}$, and for a square lattice with $\Delta x = \Delta z$, we obtain

$$\begin{aligned}
\frac{\partial D}{\partial x} &\approx \sum_\alpha c_\alpha D(x + \Delta x_\alpha, z + \Delta z_\alpha) \\
&= c_0 D(x, z) + c_1 D(x + \Delta x, z) + c_2 D(x - \Delta x, z) + c_3 D(x, z + \Delta z) + c_4 D(x, z - \Delta z) \\
&\quad + c_5 D(x + \Delta x, z + \Delta z) + c_6 D(x - \Delta x, z - \Delta z) + c_7 D(x + \Delta x, z - \Delta z) + c_8 D(x - \Delta x, z + \Delta z) \\
&= c_0 D(x, z) + c_1 \left(D(x, z) + \Delta x \frac{\partial D}{\partial x} + \frac{\Delta x^2}{2!} \frac{\partial^2 D}{\partial x^2} + O(\Delta x^3) \right) + c_2 \left(D(x, z) - \Delta x \frac{\partial D}{\partial x} + \frac{\Delta x^2}{2!} \frac{\partial^2 D}{\partial x^2} + O(\Delta x^3) \right)
\end{aligned}$$

$$
\begin{aligned}
&+c_3\left(D(x,z)+\Delta z\frac{\partial D}{\partial z}+\frac{\Delta z^2}{2!}\frac{\partial^2 D}{\partial z^2}+O(\Delta x^3)\right)+c_4\left(D(x,z)-\Delta z\frac{\partial D}{\partial z}+\frac{\Delta z^2}{2!}\frac{\partial^2 D}{\partial z^2}+O(\Delta x^3)\right)\\
&+c_5\left(D(x,z)+\Delta x\frac{\partial D}{\partial x}+\frac{\Delta x^2}{2!}\frac{\partial^2 D}{\partial x^2}+\Delta z\frac{\partial D}{\partial z}+\frac{\Delta z^2}{2!}\frac{\partial^2 D}{\partial z^2}+2\frac{\Delta x\Delta z}{2!}\frac{\partial^2 D}{\partial x\partial z}+O(\Delta x^3)\right)\\
&+c_6\left(D(x,z)-\Delta x\frac{\partial D}{\partial x}+\frac{\Delta x^2}{2!}\frac{\partial^2 D}{\partial x^2}-\Delta z\frac{\partial D}{\partial z}+\frac{\Delta z^2}{2!}\frac{\partial^2 D}{\partial z^2}+2\frac{\Delta x\Delta z}{2!}\frac{\partial^2 D}{\partial x\partial z}+O(\Delta x^3)\right)\\
&+c_7\left(D(x,z)+\Delta x\frac{\partial D}{\partial x}+\frac{\Delta x^2}{2!}\frac{\partial^2 D}{\partial x^2}-\Delta z\frac{\partial D}{\partial z}+\frac{\Delta z^2}{2!}\frac{\partial^2 D}{\partial z^2}-2\frac{\Delta x\Delta z}{2!}\frac{\partial^2 D}{\partial x\partial z}+O(\Delta x^3)\right)\\
&+c_8\left(D(x,z)-\Delta x\frac{\partial D}{\partial x}+\frac{\Delta x^2}{2!}\frac{\partial^2 D}{\partial x^2}+\Delta z\frac{\partial D}{\partial z}+\frac{\Delta z^2}{2!}\frac{\partial^2 D}{\partial z^2}-2\frac{\Delta x\Delta z}{2!}\frac{\partial^2 D}{\partial x\partial z}+O(\Delta x^3)\right)\\
&=C^{(0)}D(x,z)+C_x^{(1)}\Delta x\frac{\partial D}{\partial x}+C_z^{(1)}\Delta z\frac{\partial D}{\partial z}+C_{xx}^{(2)}\Delta x^2\frac{\partial^2 D}{\partial x^2}+C_{zz}^{(2)}\Delta z^2\frac{\partial^2 D}{\partial z^2}+C_{xz}^{(2)}\Delta x\Delta z\frac{\partial^2 D}{\partial x\partial z}+O(\Delta x^3),
\end{aligned}
\tag{23}
$$

where coefficients $C_i^{(n)}$ are coefficients of c_i grouped such that they are applied to the order (n) derivative over the i axis (axes). For the above approximation to yield the partial derivative $\partial D/\partial x$, we must solve for c_α such that $C^{(0)}=0$, $C_x^{(1)}=1/\Delta x$, $C_z^{(1)}=0$, $C_{xx}^{(2)}=0$, $C_{zz}^{(2)}=0$, and $C_{xz}^{(2)}=0$. This leads to a set of six equations with nine unknowns. However, it is well known in finite differences that use of a function value at the central point x to compute a derivative centered on x will lead to larger errors of order $O(\Delta x)$ whereas use of centered differences leads to a scheme that is accurate to order $O(\Delta x^2)$. As such, we can immediately set

$$c_0=c_3=c_4=0, \tag{24}$$

which leaves a total of five equations with six unknowns which are $C_x^{(1)}=1/\Delta x$ or

$$c_1-c_2+c_5-c_6+c_7-c_8=\frac{1}{\Delta x}, \tag{25}$$

which ensures the approximation yields the first derivative with respect to x, $C^{(0)}=0$ or

$$c_1+c_2+c_5+c_6+c_7+c_8=0, \tag{26}$$

which annuls the $D(x,z)$ terms and the Δx^2 terms, $C_z^{(1)}=0$ or

$$c_5-c_6-c_7+c_8=0, \tag{27}$$

which annuls the Δz terms, $C_{zz}^{(2)}=0$ or

$$c_5+c_6+c_7+c_8=0, \tag{28}$$

which annuls the Δz^2 terms, and $C_{xz}^{(2)}=0$ or

$$c_5+c_6-c_7-c_8=0, \tag{29}$$

which annuls the $\Delta x\Delta z$ terms. Subtracting Eq. (28) from Eq. (26) yields

$$c_1=-c_2. \tag{30}$$

Adding Eqs. (28) and (29) yields

$$c_6=-c_5. \tag{31}$$

Adding Eqs. (27) and (29) yields

$$c_7=c_5. \tag{32}$$

Finally, inserting the results of Eq. (31) and (32) into Eq. (28) yields

$$c_8=-c_5. \tag{33}$$

In other words, coefficients along the Cartesian axes are related through $c_1=-c_2$, and the coefficients along the diagonals are related through $c_5=-c_6=c_7=-c_8$. Substituting the coefficients along the Cartesian x axis denoted $c_c=c_1=-c_2$ and diagonals denoted $c_d=c_5=c_7=-c_6=-c_8$ into Eq. (25), we obtain

$$2c_c+4c_d=\frac{1}{\Delta x}. \tag{34}$$

The finite-difference approximation obtained by computing the color gradient with Eq. (22) is accurate to second order in Δx since the error is equal to that of the coefficients $c_c\propto 1/\Delta x$ and $c_d\propto 1/\Delta x$ multiplied by that of the errors in Eq. (23) of order $O(\Delta x^3)$, i.e., the error in the color-gradient calculation is of order $\Delta x O(\Delta x^3)=O(\Delta x^2)$. A similar development can be used to calculate the vertical derivative of the color difference field D. Making use of our definition of the lattice vectors $\mathbf{c}_\alpha$, we can write the color-gradient calculation in a form comparable to the standard form of

$$
\begin{aligned}
\mathbf{F}&=\sum_\alpha b_\alpha\mathbf{c}_\alpha[\rho_1(\mathbf{x}+\mathbf{c}_\alpha\Delta t,t)-\rho_2(\mathbf{x}+\mathbf{c}_\alpha\Delta t,t)]\\
&=\sum_\alpha b_\alpha\mathbf{c}_\alpha D(\mathbf{x}+\mathbf{c}_\alpha\Delta t,t),
\end{aligned}
\tag{35}
$$

where the b_α are the coefficients with $b_1=b_2=c_c=c_1=-c_2$ and $b_5=b_6=b_7=b_8=c_d=c_5=c_7=-c_6=-c_8$ that obey Eq. (34). Hence, we can see that the standard color-gradient calculation assumes $c_c=c_d=1$ (with $\Delta x=1$) which means that it computes a second order accurate finite-difference derivative of the color difference field $D=\rho_1-\rho_2$ scaled by a factor of 6. The factor of 6 is ignored in the standard color-gradient formula given by Eq. (14) as this scale factor is effectively removed by the interfacial tension parameter A which is determined for a given interfacial tension through numerical experiments and application of the Young-Laplace formula. From the development above, one may choose to weight the diagonal nearest neighbors relative

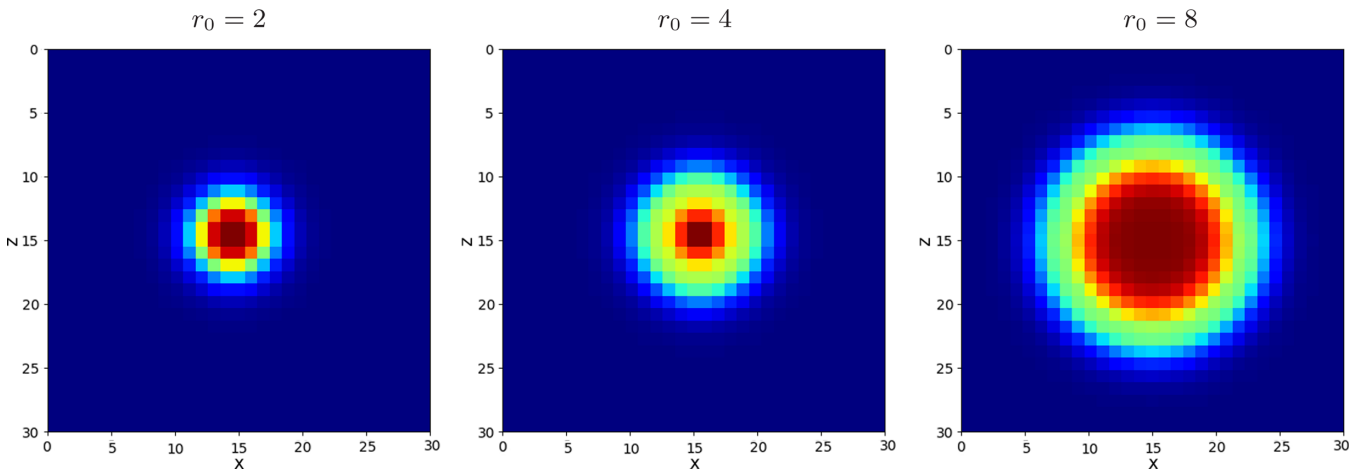

FIG. 2. Snapshots of color difference $D = (\rho_r - \rho_b)$ for small droplets of red fluid with three different radii of 2, 4, and 8 from left to right.

to the Cartesian nearest neighbors by any factor w so we can write

$$c_d = w c_c, \tag{36}$$

and once a choice of the diagonal weighting w is made, one can apply the above formulas to derive all of the coefficients b_α as will be further detailed in the next section. Hence, the important feature of the above derivation is to show that the standard color-gradient formula is not a unique way to calculate the color gradient to second order accuracy. One can choose to give no weighting to the function values along the diagonals and still obtain a second order accurate scheme by choosing $c_d = 0$ (i.e., $w = 0$). This choice is equal to a standard finite-difference approximation taking the finite differences along Cartesian axes. Or one may choose to weight the diagonal nearest neighbors equally as the Cartesian nearest neighbors (i.e., $c_c = c_d$ or $w = 1$) which is equivalent to the standard color-gradient calculation. Or one may choose an intermediate value and give less weight to the diagonals in the derivative calculation such as by setting $c_d = c_c/4$. Once the relative weight of the nearest neighbors along diagonals compared to nearest neighbors along the Cartesian axes is selected, one can calculate the values of c_c and c_d using Eq. (34). Leclaire *et al.* [21] derived a value of $w = 0.25$ in order to achieve isotropy of the finite-difference errors to second order, thereby obtaining a more isotropic color gradient and, consequently, more isotropic surface tension than is achieved using the standard color-gradient calculation of Eq. (14) which corresponds to use of $w = 1$ in Eq. (36). In the following, we will study in detail the anisotropic errors in the color gradient for small radius of curvature interfaces over the full range of possible weights $w \in [0, 1]$ which spans the original color-gradient calculation ($w = 1$), through Leclaire *et al.*'s value ($w = 0.25$), through to standard Cartesian finite differences ($w = 0$).

IV. ACCURACY AND ISOTROPY OF THE PROPOSED COLOR-GRADIENT CALCULATION

In the previous section, we have presented a general formula for the color-gradient calculation that is accurate to second order given by

$$\begin{aligned}\mathbf{F} &= \sum_\alpha b_\alpha \mathbf{c}_\alpha [\rho_1(\mathbf{x} + \mathbf{c}_\alpha \Delta t, t) - \rho_2(\mathbf{x} + \mathbf{c}_\alpha \Delta t, t)] \\ &= \sum_\alpha b_\alpha \mathbf{c}_\alpha D(\mathbf{x} + \mathbf{c}_\alpha \Delta t, t),\end{aligned} \tag{37}$$

where b_α are coefficients given by

$$b_\alpha = \begin{cases} \frac{1}{W} & \alpha = 1, 2, 3, 4 \\ \frac{w}{W} & \alpha = 5, 6, 7, 8 \end{cases}, \tag{38}$$

and the scale factor W is given by

$$W = 2 + 4w, \tag{39}$$

and the free parameter w is chosen such that

$$w \in [0, 1], \tag{40}$$

which defines how much weight is put onto the nearest neighbors along the diagonals in the finite-difference calculation of $\mathbf{F}$ relative to the nearest neighbors along the Cartesian axes. For example, a value of $w = 1$ means that the nearest neighbors along diagonals have equal weight relative to nearest neighbors along the Cartesian axes, which corresponds to the standard (original) way in which the color gradient $\mathbf{F}$ is calculated as per Eq. (14) as defined by Latva-Kokko and Rothman [17]. Note that the factor W scales the coefficients b_α such that the calculation of $\mathbf{F}$ yields the color gradient, whereas the standard color-gradient calculation yields six times the actual color gradient.

Like any finite-difference calculation, the accuracy of the color-gradient calculation has an accuracy that depends on (1) the smoothness of the function the derivative of which is being calculated which relates to the RK LBM interface thickness parameter β and (2) the radius of curvature of the interface. In the following, we set the interface thickness parameter to $\beta = 0.5$ which is the value that is typically used in the RK LBM, and study the accuracy of the color-gradient calculation for three different radii of curvature of the interface. It is expected that as the radius of a droplet decreases, the accuracy of the color-gradient calculation will decrease. A square region of blue fluid was initialized containing a circular region of the red fluid within specified radii of $r_0 = 2, 4$, and

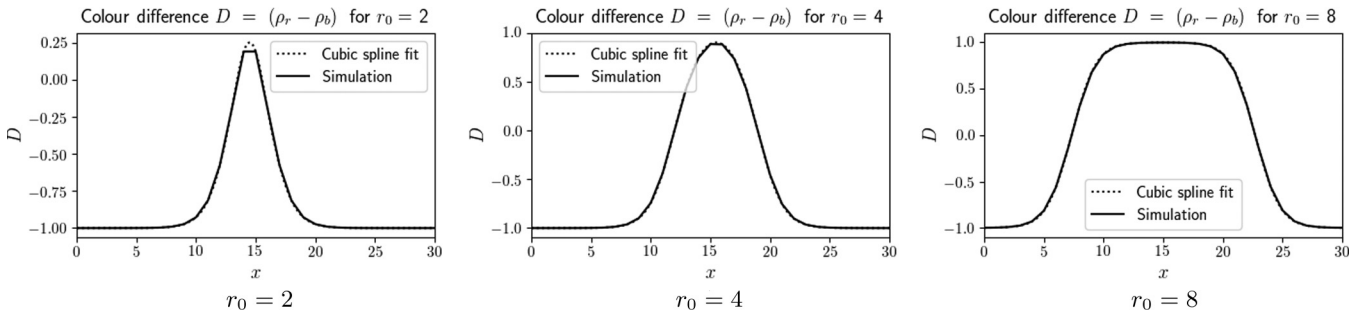

FIG. 3. Plots of color difference $D(x, z_0) = (\rho_r - \rho_b)(x, z_0)$ and cubic spline fits of the droplets with three different radii of $r_0 = 2$, 4, and 8 from left to right.

8, and LBM simulations were performed until the fluid droplet and interface stabilized. Figure 2 shows the color difference $D = (\rho_r - \rho_b)$ after the simulations stabilized. To study the accuracy of the finite-difference calculation of the color gradient, we fit the color difference $D = (\rho_r - \rho_b)$ using cubic splines for the three cases being studied with $r_0 = 2, 4$, and 8. Figure 3 shows plots of the color difference in the LBM taken through the center of the droplet at $z = z_0$, along with the cubic spline fits of the color difference. These spline fits are used to calculate a radially symmetric color difference field for each of the three cases.

In the following, we compute the color gradient numerically from the radially symmetric spline fits of the color difference field for the three different radii of droplets $r_0 = 2, 4$, and 8 using three different values of w in Eqs. (37)–(39). Specifically, we use values of $w = 1$ which yields the color gradient calculated in the standard way, $w = 0$ which corresponds to using finite differences along the Cartesian axes, and an intermediate value of $w = 0.25$, the value derived by Leclaire *et al.* that yields isotropic errors to second order [21]. The anisotropic errors in the three numerical color-gradient calculations are then compared and analyzed.

Figure 4 shows the normalized color gradient defined as

$$F(w) = \frac{|\mathbf{F}(w)|}{\max[|\mathbf{F}(w)|]}, \tag{41}$$

for the three different droplet radii computed numerically using Eqs. (37)–(39). One observes that for the smallest radius droplet ($r_0 = 2$), the color gradient computed with $w = 1$ is anisotropic with higher values along the diagonals compared to along the Cartesian axis directions. In contrast, for the case with $w = 0$, the color gradient is also anisotropic but has higher values along the Cartesian axes. For the intermediate case of $w = 0.25$, the plot of the color gradient appears to be almost isotropic. For the case of $r_0 = 4$, a similar anisotropic effect can be seen but it is significantly reduced, and for the case of $r_0 = 8$, the plots appear to be isotropic.

To enable the anisotropy in the color gradient to be better visualized, we define the anisotropic error $E(w)$ as the difference between the normalized color gradient $F(w)$ and an isotropic color-gradient field. Namely, we define r as the distance between point (x, z) and the center of a droplet $r = \sqrt{(x - x_0)^2 + (z - z_0)^2}$, and θ as the angle so $(x - x_0) = r\cos(\theta)$ and $(z - z_0) = r\sin(\theta)$ where the droplet is centered at (x_0, z_0). We define the anisotropic error relative to the color gradient at angle $\theta = 0$ as

$$E_{r,\theta}(w) = \frac{F_{r,\theta}(w) - F_{r,0^\circ}}{\max(F_{r,0^\circ})}. \tag{42}$$

Hence, this color-gradient error will highlight any anisotropy in the numerical color-gradient field. A value of $E(w) > 0$ means that the color gradient at that angle is higher than along the Cartesian axes, and a value of $E(w) < 0$ means that the color gradient at that angle is lower than the color gradient along Cartesian axes. Figure 5 shows the anisotropic error plotted in the space domain for the three droplet sizes, and for three values of the free parameter w. These plots indicate that using the standard color-gradient calculation ($w = 1$), the maximum anisotropic error is significant with around 7% higher color-gradient values along the diagonals for the smallest radius example ($r_0 = 2$). Similarly, if one uses Cartesian finite differences to calculate the color gradient ($w = 0$), the maximum anisotropic error is also significant with over 7% lower color-gradient values along the diagonals (i.e., higher color gradient along Cartesian axes). Again, the color gradient calculated using the intermediate value of $w = 0.25$ had much lower anisotropy, being only of order -1.4%.

To further study how the parameter w impacts on the anisotropy of the numerical color gradient, we compute the maximum anisotropy for a range of w values ranging from $w = 1$ down to $w = 0$ for each of the three droplet radii ($r_0 = 2$, 4, and 8). Figure 6 shows the anisotropy as a function of w where maximum anisotropy is defined as

$$A = \text{anisotropy} = \text{sign}[E_{r^*,45^\circ}(w) - E_{r^*,0^\circ}(w)] \times \max_r |E_{r,45^\circ}(w) - E_{r,0^\circ}(w)|, \tag{43}$$

where r^* is the radius where the highest anisotropy is found. Figure 6 shows the maximum anisotropy as a function of w for the three different droplet radii r_0. These calculations indicate that for the case of $r_0 = 2$, the anisotropy is minimized at a value of $w = 0.298$ and at this w value, the anisotropy is only -0.66%. At this value of w, the anisotropy for the cases of $r_0 = 4$ and 8 is 0.24 and 0.22%. The optimal value of w for the case of $r_0 = 4$ is $w = 0.28$ with a maximum anisotropy of 0.16%, and the optimal w for the case of $r_0 = 8$ is $w = 0.271$ with a maximal anisotropy of 0.13%. Based on these results, we propose an optimal w value which minimizes anisotropy

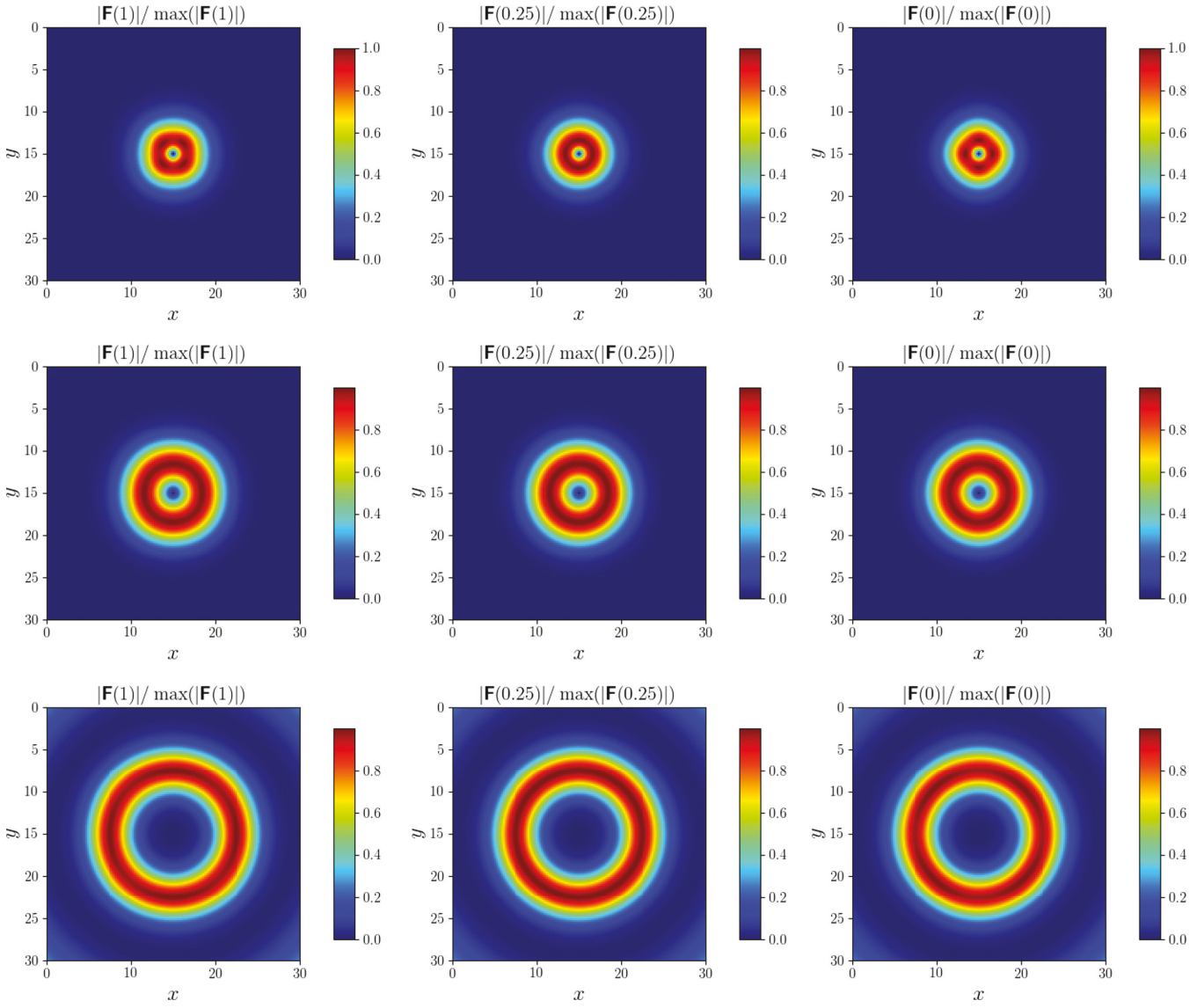

FIG. 4. Plots of the normalized color gradient calculated using Eqs. (37)–(39) for three different radii of droplets r_0 and three different values of w. From left to right: Color gradient (CG) using $w = 1$ (original CG calculation), calculation using $w = 0.25$ (diagonals weighted down by a factor of $w = 0.25$), and calculation using $w = 0$ (CG via finite differences along coordinate axes). From top to bottom: Smallest radius ($r_0 = 2$), middle radius ($r_0 = 4$), and largest radius ($r_0 = 8$).

of

$$w_{\text{optimal}} = 0.298 \sim 0.3. \tag{44}$$

Setting $w = 0.298$ leads to a maximum magnitude of anisotropy of 0.66, 0.24, and 0.22%, respectively, for the cases of $r_0 = 2, 4$, and 8. Using the proposed optimal value of $w_{\text{optimal}} = 0.298$, the anisotropy in the numerical color gradient is less than 0.7% for all values of r_0 tested, an improvement of over a factor of 10 less anisotropy relative to the standard color-gradient calculation. Note that the reason we selected the larger value of $w_{\text{optimal}} = 0.298$ which minimized anisotropy of the $r_0 = 2$ droplet is because we anticipate that phenomenology such as fingering and droplet formation initiates at the smallest scale and hence the lowest r_0. Hence, we wish to maximize isotropy for these small scale phenomena. Also, the anisotropy of the larger radii droplets remains below the anisotropy of the $r_0 = 2$ droplet at a value of $w = 0.298$. This choice of w achieves the highest accuracy at the lowest r_0 and is the best choice if the goal is for the Rothman-Keller color-gradient lattice Boltzmann method to yield the most realistic phenomenology at the smallest scales. Note that the sharp jump down from 0.66 to −0.66% anisotropy at $w = 0.298$ for the $r_0 = 2$ droplet shows that for $w > 0.298$ the maximum anisotropy is positive (i.e., diagonals have higher color-gradient values than along the Cartesian axes), whereas for $w < 0.298$, the maximum anisotropy is negative (i.e., diagonals have lower color gradient than along the Cartesian axes). It is interesting to note that the maximum anisotropy for the standard color-gradient calculations with $w = 1$ does not occur where the color gradient is maximal. Figure 7 shows the anisotropy for the smallest droplet with $r_0 = 2$ for cases of $w = 1$ (original CG formula) and $w = 0.298$ (optimal w that minimizes anisotropy), and Fig. 8

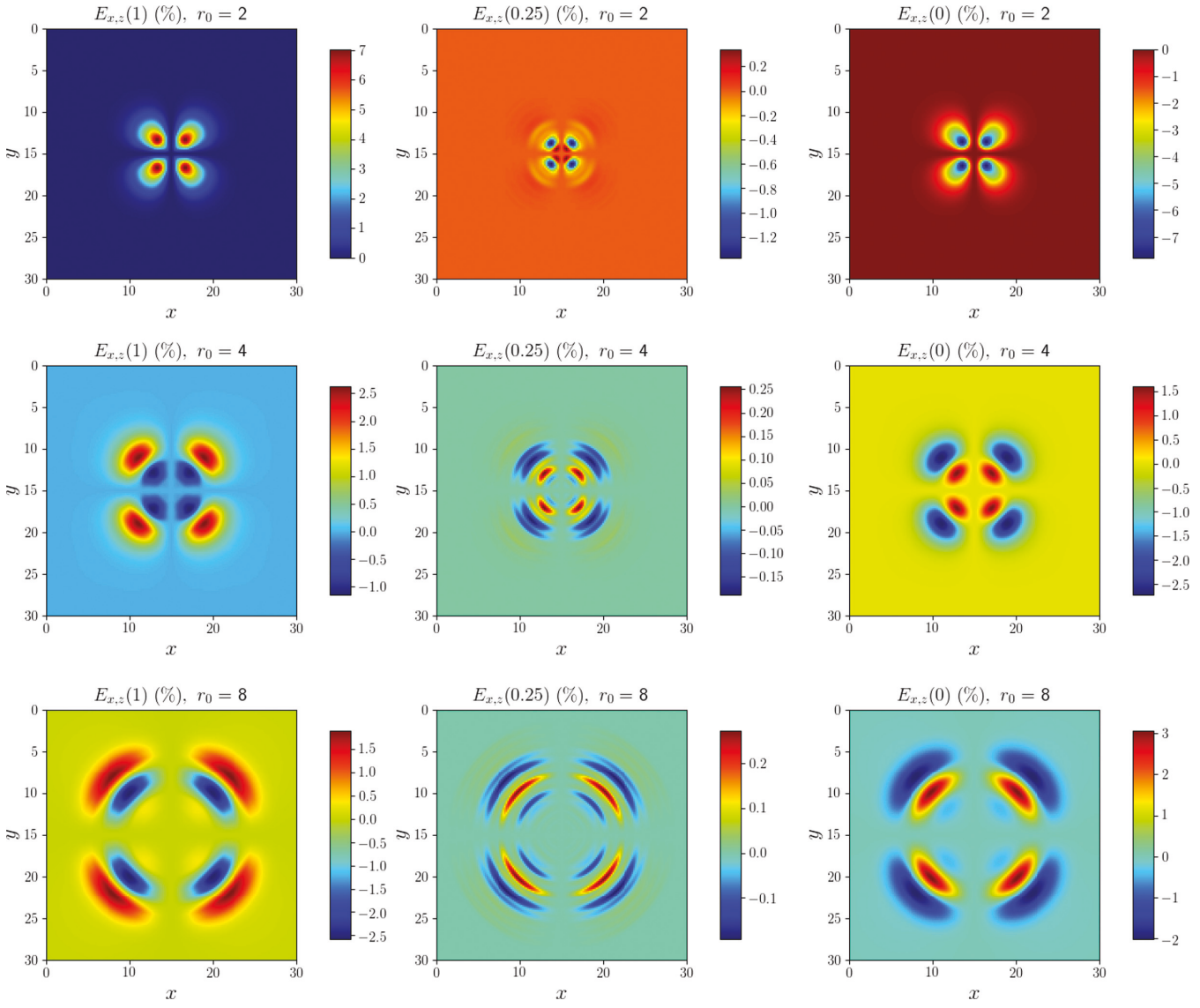

FIG. 5. Plots of the anisotropic error $E(w)$ in the space domain calculated using different values of w calculated using Eq. (42). From left to right: Error for $w = 1$ (original CG calculation), calculation using $w = 0.25$ (diagonals weighted down by a factor of $w = 0.25$), and calculation using $w = 0$ (CG via Cartesian finite differences). From top to bottom: Smallest radius ($r_0 = 2$), middle radius ($r_0 = 4$), and largest radius ($r_0 = 8$).

shows the anisotropy at the radius of maximal anisotropy for the smallest droplet with $r_0 = 2$ for the cases of $w = 1$ and 0.298.

To illustrate the anisotropy for the optimal value of $w = 0.298$, we plot the anisotropic error for this value of w in Fig. 9. These plots show that there is both positive and negative anisotropic error at the optimal value of $w = 0.298$ at different radii, and that the magnitude of the maximum error is less than about 0.6%. It is logical to assume that the positive anisotropic error along diagonals at the higher radii will in part cancel the effect on surface tension of the negative anisotropic error along diagonals at lower radii, so in Fig. 10, we plot the weighted mean anisotropic error as a function of angle for the smallest radius droplet $r_0 = 2$ which is defined as

$$\bar{E}_\theta(w) = \frac{\sum_r F_{r,0^\circ} E_{r,\theta}}{\sum_r F_{r,0^\circ}}, \tag{45}$$

where the anisotropic error is weighted by the normalized color gradient along the Cartesian axes $F_{r,0^\circ}$. We also define the maximum mean anisotropic error as the mean anisotropic error at 45°, so we have

$$\bar{A} = \text{mean anisotropy} = \bar{E}_{r,45^\circ}. \tag{46}$$

This plot indicates that the mean anisotropic error for the optimal case of $w = 0.298$ is around 0.12%, about 34 times lower than the mean anisotropic error of 4.24% for the standard color-gradient calculation with $w = 1$. To see the detail of how the color-gradient error depends on the radius r, we plot in Fig. 11 the anisotropic error at 45° together with the color gradient for the two cases of $w = 1$ (original CG calculation) and $w = 0.298$ (optimal w that minimizes anisotropy). Note that in the plot, the color gradient is scaled by factors of s_1 and s_2 to enable the shape of the CG to be visualized on the same plot as the anisotropic error. One observes that for

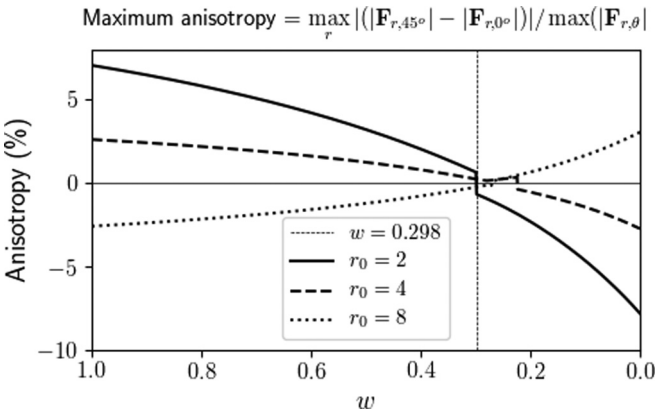

FIG. 6. Plots of the maximum anisotropy vs w for three different radii r_0 of a droplet.

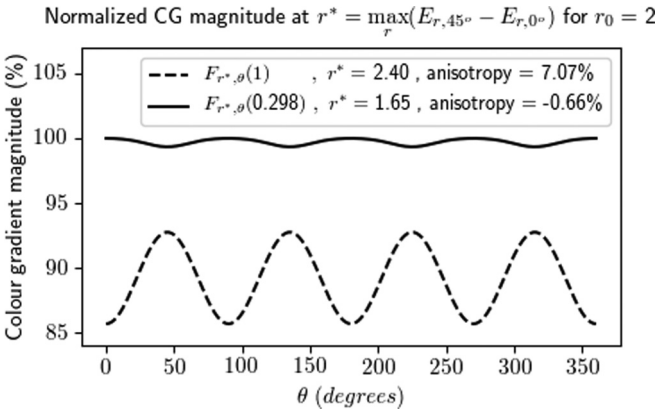

FIG. 8. Plots of the normalized color gradient as a function of direction θ at the radius of maximal anisotropy $r^* = \max_r E_{r,45^\circ} - E_{r,0^\circ}$ for the original color-gradient calculation ($w = 1$) and the proposed optimal value of $w = 0.298$ for the smallest droplet with $r_0 = 2$.

$w = 1$, the maximal anisotropic error is about 7% and occurs at a significantly higher radius of $r^* = 2.4$ than the radius of maximal color gradient of $r_F = 1.65$. In contrast, the maximal anisotropic error of -0.66% for the optimal value of w occurs at the radius of the maximum color gradient of $r_F = 1.65$.

Figure 12 shows the set of plots of anisotropic error for the case of $w = 0.25$ (the value derived by Leclaire *et al.* [21]) for the smallest radius of droplet with $r_0 = 2$ for comparison with the same plots for the optimal value of $w = 0.298$ shown in Figs. 7, 8, 10, and 11. The plots for the case of $w = 0.25$ have a significantly higher anisotropic error than the plots for the optimal case of $w = 0.298$. Specifically, use of the value of $w = 0.25$ in the color-gradient calculations yields a maximum anisotropic error of 1.38% compared to a maximum error of 0.66% obtained when using the optimal value of $w = 0.298$, about two times larger. Furthermore, the mean anisotropic error is significantly higher using $w = 0.25$ having a value of 0.37% compared to 0.12% for the case of the optimal weight of $w = 0.298$, which is about three times larger. Considering that it is logical to assume that some of the effect of the too high color gradient at certain r will negate the effect of the too

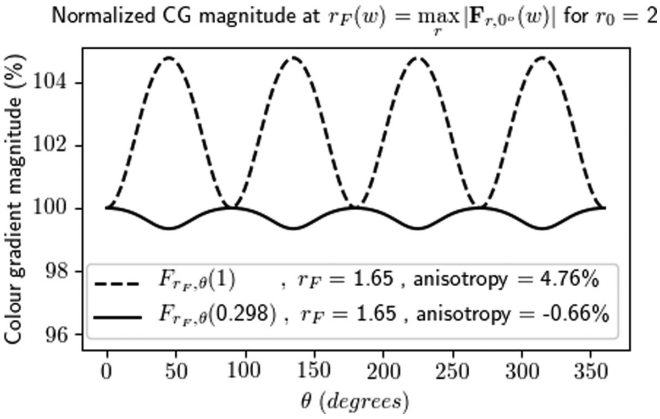

FIG. 7. Plots of the normalized color gradient as a function of direction θ at the radius of maximal color gradient $r_F = \max_r F_{r,0^\circ}(w)$ for the original color-gradient calculation ($w = 1$) and the proposed optimal value of $w = 0.298$ for the smallest droplet with $r_0 = 2$.

low color gradient at different r, it is reasonable to conclude that in practice, the factor improvement using the proposed value of $w = 0.298$ is 2 to 3. Figure 13 shows the anisotropic error in the space domain for the value of $w = 0.25$ for comparison with the anisotropic error for the optimal case of $w = 0.298$ shown in Fig. 9.

V. ANISOTROPY SUMMARY AT DIFFERENT VALUES OF SMOOTHING PARAMETER β

So far, we have focused on analyzing the case where the interface smoothing parameter is $\beta = 0.5$ which is widely used in the literature. However, as the smoothing parameter impacts the shape and sharpness of the fluid interface which implies it will also affect the accuracy of the finite-difference calculations, it is also interesting to compute the anisotropy for different typical cases of β such as $\beta = 0.7$ and 0.99 [21]. Note that the viscosity ratio $M = \nu_r/\nu_b$ and interfacial tension parameter A do not significantly affect the shape of the interface which is entirely controlled by the recoloring step and, hence, the parameter β. To demonstrate this, we calculated the optimal value of w denoted w_{opt} for various A in the range $A \in [0.1, \ldots, 10^{-13}]$ with $\nu_r = \nu_b = 0.02$, and for the case of a viscosity ratio of $M = \nu_r/\nu_b = 0.01$ with $\nu_r = 0.002$, $\nu_b = 0.2$. The results are shown in Table I and demonstrate that w_{opt} is insensitive to A and the viscosities and viscosity ratio. Table II contains a summary of the anisotropy defined by Eq. (43), the weighted mean anisotropy defined in Eq. (46), and the factor improvement in isotropy relative to the cases of $w = 1$ and Leclaire's value of $w = 0.25$. The table summarizes the anisotropic error for each $\beta = (0.5, 0.7, 0.99)$ and for each radius of curvature $r_0 = (2, 4, 8)$.

From Table II, we see that for $\beta = 0.5$, the anisotropy using the proposed optimal weight $w = 0.298$ for $r_0 = 2$ droplets is $A = 0.66\%$ which is 10.8 times lower than the anisotropy using the standard weight of $w = 1$ and 2.1 times lower than the anisotropy using Leclaire's weight of $w = 0.25$. And the mean anisotropic error is only $\bar{A} = 0.12\%$ which is 34.2 times lower than using the standard w value, and 3.2 times smaller

TABLE I. Optimal w at various A and at a viscosity ratio of $M = \nu_r/\nu_b = 0.01$ showing insensitivity of w_{opt} to A and viscosity ratio.

r_0	$A = 0.1$	$A = 0.01$	$A = 10^{-12}$	$A = 10^{-13}$	$\nu_r = 0.002$, $\nu_b = 0.2$
2	0.299	0.298	0.298	0.298	0.298
4	0.282	0.280	0.279	0.279	0.282
8	0.269	0.270	0.270	0.270	0.270

than using Leclaire's w value. For the higher radii droplets, the factor improvement over the standard w value is also high ($\approx$10), but the factor improvement over the standard Leclaire is only slight. However, one should note that in any event, the anisotropy is much lower for the higher radii of curvature, being $A \leqslant 0.24\%$ in both cases (i.e., 2.75 times less than for the $r_0 = 2$ case). As such, the anisotropic error at the lowest radius of curvature is the dominant source of error, and also has the most impact on fingering and pinchout transitions. For this reason, we recommend use of the optimal w value of $w = 0.298$ at $r_0 = 2$ in Table II for the case of $\beta = 0.5$, especially for studies of fingering and pinchout transitions.

Similarly, from Table II, we see that for $\beta = 0.7$, the anisotropy using the proposed optimal weight of $w = 0.284$ for $r_0 = 2$ droplets is only 0.35%, which is about 18 times lower than the anisotropy using the standard weight, and about 1.8 times lower than the anisotropy using Leclaire's weight of $w = 0.25$. And the mean anisotropic error is only $\bar{A} = 0.02\%$ which is 185 times smaller than using the standard weight and about 15 times smaller than using Leclaire's value. For the higher radii of curvature droplets, the factors of improvement over the standard and Leclaire cases are, respectively, over 13 and over 2. At these higher radii of curvature, the magnitude of the anisotropy is only slightly lower than the anisotropy for the $r_0 = 2$ case, being less than 0.3%.

Finally, from Table II, we see that for $\beta = 0.99$, the anisotropy using the proposed optimal weight of $w = 0.275$ for $r_0 = 2$ droplets is only 0.67%, which is more than 11 times lower than the anisotropy using the standard weight of $w = 1$, and is about 1.7 times lower than the anisotropy using Leclaire's weight of $w = 0.25$. Here, the mean anisotropic error is very low at $\bar{A} \sim 0.09\%$ which is about 33 times less than using the standard w value, and about 1.1 times less than the mean anisotropic error using Leclaire's value. At this highest value of $\beta = 0.99$, the higher radii of curvature cases have an anisotropic error of about 1%. At these higher radii of curvature, the proposed weight leads to about six times less anisotropic error than using the standard weight, and a slight factor 1.3 improvement relative to using Leclaire's weight.

In summary, from Table II, at the smallest radius droplet of $r_0 = 2$ which is the radius that will have the dominant effect on controlling fingering and pinchout transitions, the proposed optimal values of w for each of $\beta = 0.5$, 0.7, and 0.99, dramatically outperform the standard color-gradient calculations by a factor of around 11–18, and offer a factor of around 2 lower anisotropy than Leclaire's value of $w = 0.25$. The mean anisotropy is also much lower using the proposed w values than using the standard calculations, being a factor of 33–185 lower. Relative to using Leclaire's w value, the mean anisotropy ranges from 15 times lower for $\beta = 0.7$, to 3.2 times lower for $\beta = 0.5$, to just 1.1 times lower for the case of $\beta = 0.99$.

For all three β values, using the recommended values of w, namely, the optimal w at the lowest value of $r_0 = 2$, leads to less than 0.67% anisotropy and less than about 0.1% average anisotropy. Specifically, for $\beta = (0.5, 0.7, 0.99)$, the anisotropy is $A = (0.66\%, 0.35\%, 0.67\%)$ and the mean anisotropy is $\bar{A} = (0.12\%, 0.02\%, 0.085\%)$. This compares to anisotropy of 6–7% for the standard value of $w = 1$ and about 3–4% average anisotropy. And for Leclaire's $w = 0.25$ value, the anisotropy for the three β values is $A = (1.38\%, 0.62\%, 1.15\%)$ and the mean anisotropy is $\bar{A} = (0.4\%, 0.32\%, 0.09\%)$.

Based on the above and considering that it is the lowest radii of curvature that have both the highest anisotropic error and the most significant impact on transitions such as fingering and droplet formation, we recommend the use of the $r_0 = 2$ optimal w values of $w = (0.298, 0.284, 0.275)$, respectively, for the cases of $\beta = (0.5, 0.7, 0.99)$ when using the Rothman-Keller color-gradient LBM to model complex pore scale processes and related transitions.

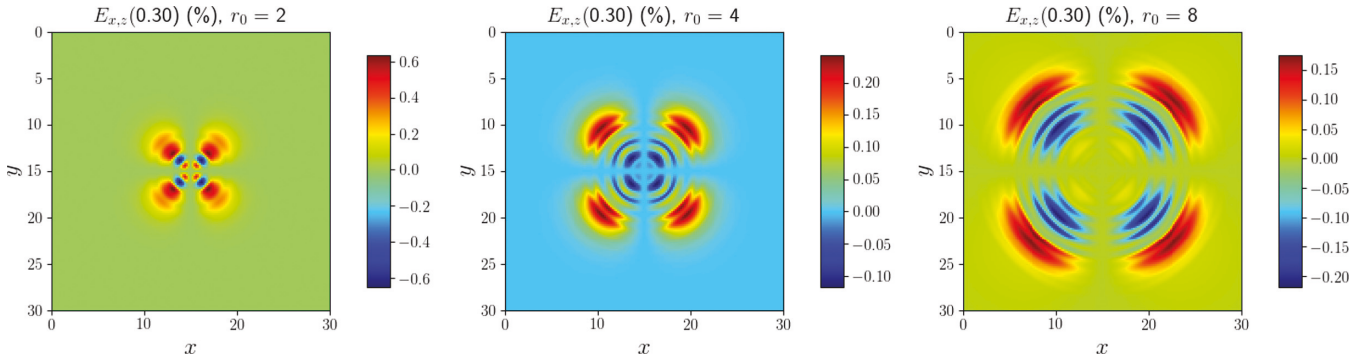

FIG. 9. Plots of the anisotropic error $E(w)$ in the space domain calculated using the proposed optimal value of $w = 0.298$. From left to right: Error for $r_0 = 2$, 4, and 8.

TABLE II. Comparison of the anisotropic error A and mean anisotropic error $\bar{A}$ in percent, and the corresponding factor decrease in anisotropic error and mean error relative to the standard and Leclaire's $w = 0.25$ case. The bold lines represent use of the choice of w that is optimal for the smallest radius of curvature droplet with $r_0 = 2$, which are the recommended optimal w values for each β.

				Anisotropy (%)		Factor less than standard		Factor less than Leclaire	
β	r_0	What	w	A	$\bar{A}$	$A(1)/A(w)$	$\bar{A}(1)/\bar{A}(w)$	$A(0.25)/A(w)$	$\bar{A}(0.25)/\bar{A}(w)$
0.5	2	Standard	1	7.07	4.24	1.00	1.00	0.20	0.09
0.5	2	Leclaire	0.25	1.38	0.40	5.12	10.70	1.00	1.00
0.5	2	Optimal	0.298	0.66	0.12	10.78	34.21	2.10	3.20
0.5	4	Standard	1	2.63	0.25	1.00	1.00	0.10	0.08
0.5	4	Leclaire	0.25	0.26	0.02	10.13	12.07	1.00	1.00
0.5	4	Optimal_2	0.298	0.24	0.05	10.77	5.09	1.06	0.42
0.5	4	Optimal	0.28	0.155	0.039	16.94	6.43	1.67	0.53
0.5	8	Standard	1	2.58	0.76	1.00	1.00	0.11	0.03
0.5	8	Leclaire	0.25	0.27	0.026	9.46	29.37	1.00	1.00
0.5	8	Optimal_2	0.298	0.22	0.068	11.79	11.17	1.25	0.38
0.5	8	Optimal	0.271	0.127	0.017	20.23	45.73	2.14	1.56
0.7	2	Standard	1	6.36	3.80	1.00	1.00	0.10	0.08
0.7	2	Leclaire	0.25	0.62	0.32	10.21	12.09	1.00	1.00
0.7	2	Optimal	0.284	0.35	0.02	18.24	185.53	1.79	15.35
0.7	4	Standard	1	3.78	0.78	1.00	1.00	0.16	0.11
0.7	4	Leclaire	0.25	0.61	0.083	6.20	9.49	1.0	1.0
0.7	4	Optimal_2	0.284	0.283	0.011	13.35	73.73	2.15	7.77
0.7	4	Optimal	0.286	0.27	0.007	13.97	119.22	2.25	12.56
0.7	8	Standard	1	4.07	1.42	1.00	1.00	0.16	0.05
0.7	8	Leclaire	0.25	0.66	0.072	6.21	19.60	1.00	1.00
0.7	8	Optimal_2	0.284	0.281	0.056	14.45	25.28	2.33	1.29
0.7	8	Optimal	0.282	0.273	0.049	14.89	29.03	2.40	1.48
0.99	2	Standard	1	7.76	2.77	1.00	1.00	0.15	0.03
0.99	2	Leclaire	0.25	1.15	0.09	6.74	29.72	1.00	1.00
0.99	2	Optimal	0.275	0.67	0.085	11.55	32.78	1.71	1.10
0.99	4	Standard	1	5.86	0.52	1.00	1.00	0.23	0.48
0.99	4	Leclaire	0.25	1.33	0.25	4.40	2.07	1.00	1.00
0.99	4	Optimal_2	0.275	1.016	0.208	5.77	2.50	1.31	1.21
0.99	4	Optimal	0.299	0.74	0.17	7.92	3.08	1.80	1.49
0.99	8	Standard	1	6.08	0.4	1.00	1.00	0.22	0.66
0.99	8	Leclaire	0.25	1.36	0.26	4.47	1.52	1.00	1.00
0.99	8	Optimal_2	0.275	1.066	0.23	5.71	1.76	1.28	1.16
0.99	8	Optimal	0.303	0.76	0.19	8.01	2.12	1.79	1.40

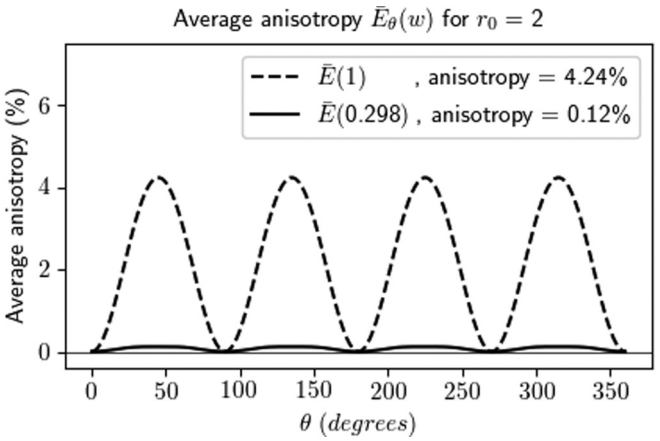

FIG. 10. Plots of the mean anisotropic error as a function of direction θ at the radius of maximal anisotropy $r^* = \max_r(E_{r,45^\circ} - E_{r,0^\circ})$ for the original color-gradient calculation ($w = 1$) and the proposed optimal value of $w = 0.298$ for the smallest droplet with $r_0 = 2$.

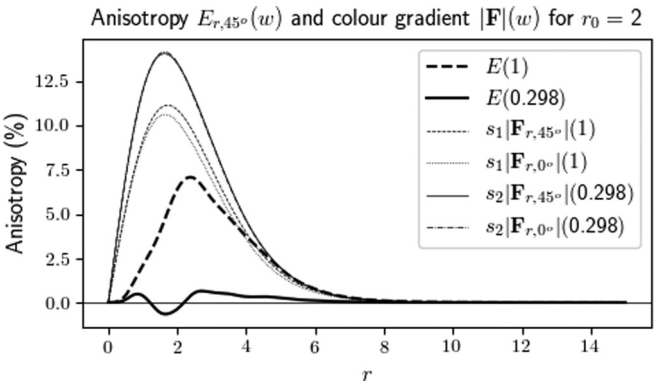

FIG. 11. Plot of the anisotropic error at 45° together with the color gradient for the two cases of $w = 1$ (original CG calculation) and $w = 0.298$ (optimal w that minimizes anisotropy) for the smallest droplet with $r_0 = 2$. The color gradient is scaled by factors of s_1 and s_2 to enable the shape of the color-gradient magnitude $|\mathbf{F}(w)|$ to be visualized on the same plot as the error.

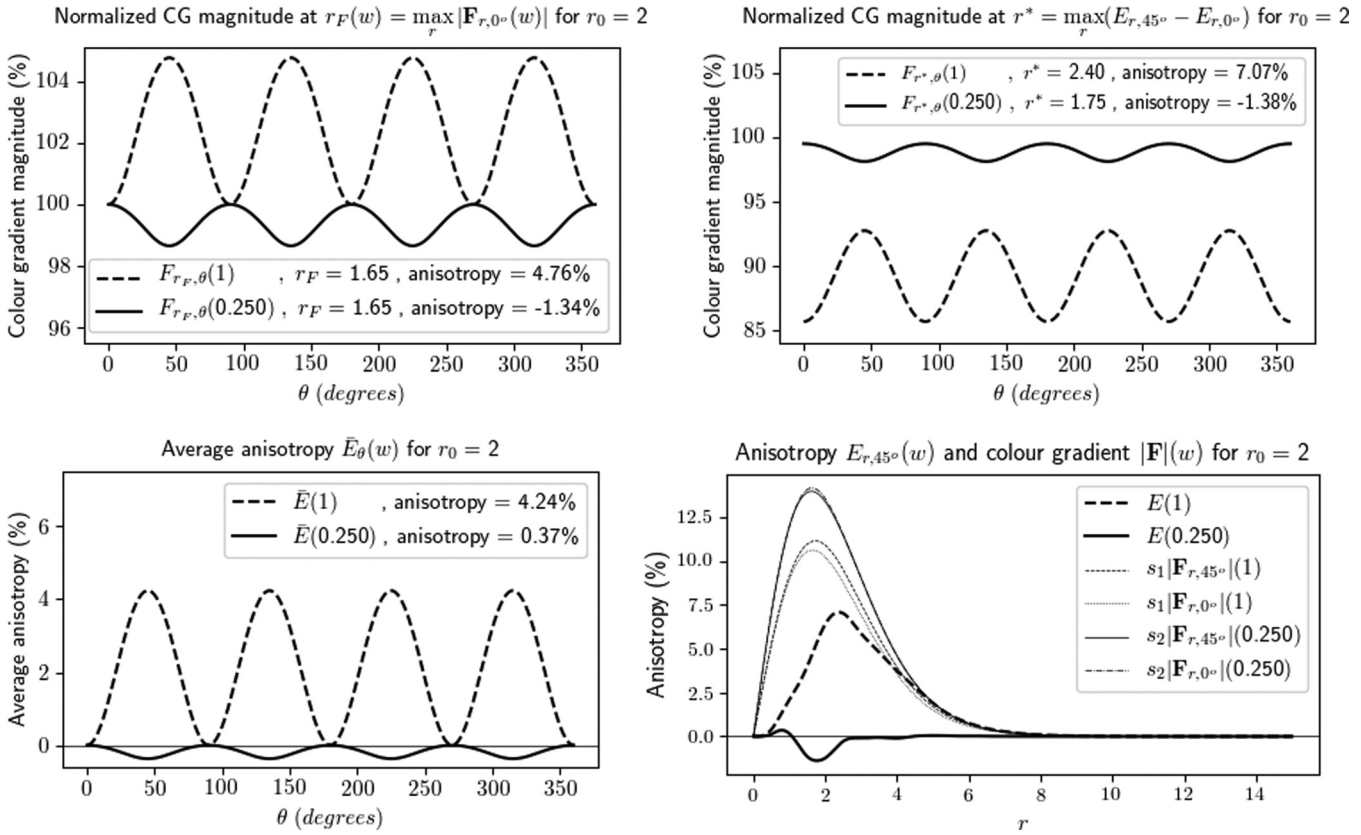

FIG. 12. Plots for the case of $w = 0.25$ for the smallest radius of droplet with $r_0 = 2$ for comparison with Figs. 7, 8, 10, and 11 which were for the optimal case of $w = 0.298$. Upper left: The normalized color gradient as a function of direction θ at the radius of maximal color gradient $r_F = \max_r F_{r,0^\circ}(w)$ for the original color-gradient calculation ($w = 1$) and the value of $w = 0.25$. Upper right: The normalized color gradient as a function of direction θ at the radius of maximal anisotropy $r^* = \max_r E_{r,45^\circ} - E_{r,0^\circ}$ for the original color-gradient calculation ($w = 1$) and the value of $w = 0.25$. Lower left: The mean anisotropic error as a function of direction θ for the original color-gradient calculation ($w = 1$) and the value of $w = 0.25$. Lower right: The anisotropic error at 45° together with the color gradient for the two cases of $w = 1$ (original CG calculation) and $w = 0.25$. The color gradient is scaled by factors of s_1 and s_2 to enable the shape of the color-gradient magnitude $|\mathbf{F}(w)|$ to be visualized on the same plot as the error.

VI. EXAMPLE OF PHENOMENA MISSED DUE TO ANISOTROPY OF THE STANDARD COLOR-GRADIENT CALCULATION

The previous section has shown that there is about a 7% anisotropic error using the standard color-gradient calculation according to Eq. (14) whereas the proposed color-gradient calculation using Eqs. (37)–(39) and a value of $w = 0.298$ leads to much lower anisotropy of approximately 0.66%. Furthermore, the proposed color-gradient calculation has both positive and negative anisotropies at different radii with a mean anisotropy of only about 0.12% (see Fig. 10) so the effect of the anisotropy of the color gradient on surface tension at $w = 0.298$ is likely to be even smaller than

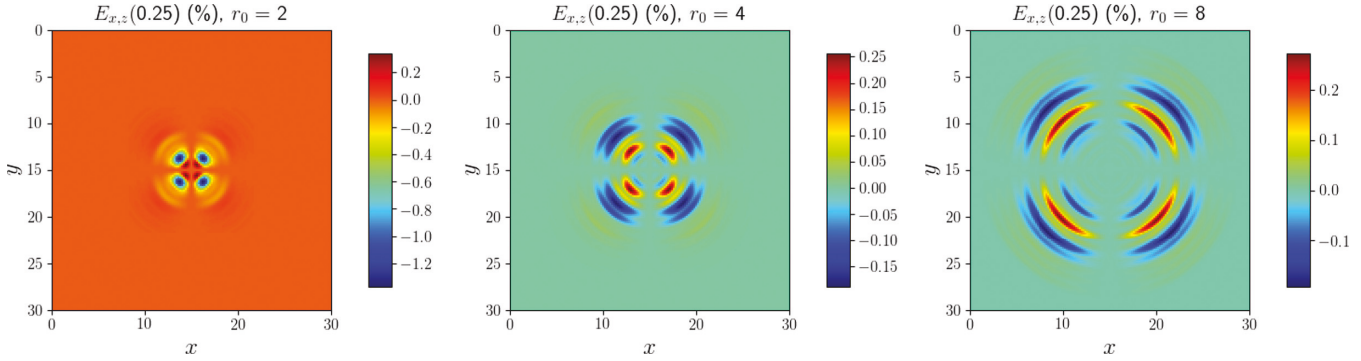

FIG. 13. Plots of the anisotropic error $E(w)$ in the space domain calculated using the value of $w = 0.25$ for comparison with Fig. 9 calculated with the optimal value of $w = 0.298$. From left to right: Error for $r_0 = 2$, 4, and 8.

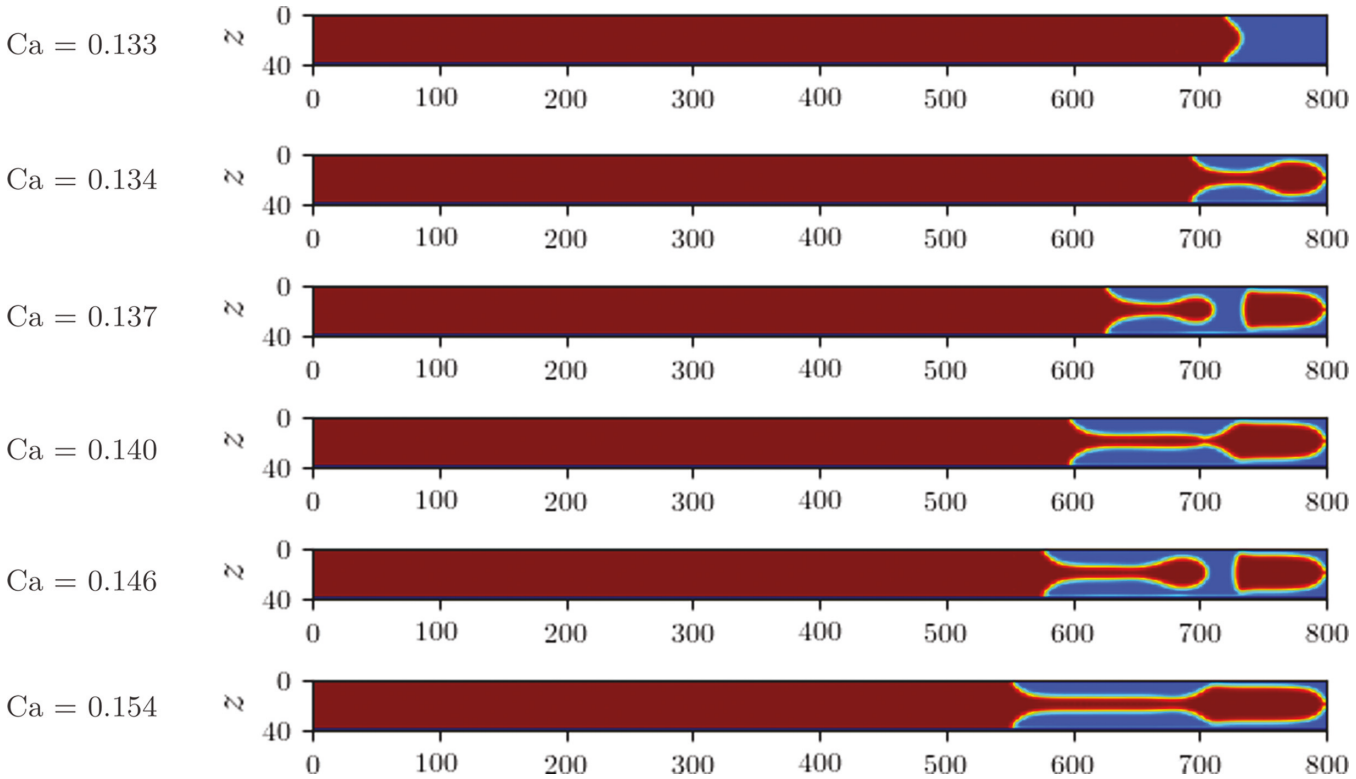

FIG. 14. Snapshots of flow in a pipe for wetting angle of $\theta = 0$ and various capillary numbers using the optimal value of $w = 0.298$ to calculate the color gradient.

suggested by the maximum anisotropy of 0.66%. The anisotropy in the color gradient will have the greatest effect for small radii of curvature of fluid boundaries such as at the pinchout when droplets form. In this section, we demonstrate that the anisotropy of the standard color gradient leads to fundamentally different results for certain cases. Specifically, we show in this section that the transition to fingering in a pipe using the standard color-gradient calculation does not lead to formation of droplets, whereas when one applies the proposed more isotropic color-gradient calculation, droplets form at the transition to fingering.

In this section, we simulate flow in a 2D pipe of length 800 and width of 40 units. A wetting red fluid with wetting angle $\theta_w = 0^\circ$ is injected from the left with a specified injection velocity, and constant pressure boundary conditions are specified at the right of the tube where these boundary conditions were calculated using the Zou and He velocity and pressure boundary conditions [30]. Numerous simulations over a range of capillary numbers were run to determine and study the transition to fingering, where capillary number is defined as

$$\mathrm{Ca} = \frac{\rho_r \nu_r u_{\mathrm{in}}}{\sigma} = \frac{\mu_r u_{\mathrm{in}}}{\sigma}, \tag{47}$$

where ν_r is the kinematic viscosity of the invading red fluid, μ_r is the dynamic viscosity of the invading red fluid, and σ is the interfacial tension which can be determined through a simulation of a static droplet and application of the Young-Laplace formula

$$\sigma = r_0 \Delta P = r_0 (P_{\mathrm{in}} - P_{\mathrm{out}}), \tag{48}$$

where ΔP is the difference in average pressure inside versus outside a droplet of radius r_0 (i.e., the radius between the drop center and the contour of $D = 0$). Note that the use of Eq. (48) effectively yields the mean surface tension where the average is over angle. So due to the anisotropy of the color-gradient calculations, the surface tension in the RK LBM may be higher or lower than this mean value depending on the angle. We find that using the proposed color-gradient calculations given by Eqs. (37)–(39), the interfacial tension is typically found to be $\sigma \in [0.55 \times A, 0.79 \times A]$ where A is the interfacial tension term specified in the second collision term given by Eq. (13). In these simulations of flow in a pipe, we fix the inlet velocity to be $u_{\mathrm{in}} = 0.02$, and we vary the interfacial tension parameter A to allow different capillary numbers to be simulated. Namely, numerous simulations were done of a static droplet at different values of A to determine the relationship between A and σ which allowed us to accurately specify each interfacial tension parameter A required to model a specific capillary number with a constant injection flow rate u_{in} using Eq. (47). The kinematic viscosities were set to $\nu_1 = \nu_2 = 0.02$ (i.e., viscosity ratio of $M = 1$). Figure 14 shows snapshots for a range of capillary numbers surrounding the transition to fingering calculated using the proposed more isotropic color-gradient calculation with $w = 0.298$, whereas Fig. 15 shows snapshots for the standard color-gradient calculation using a value of $w = 1$. We observe two fundamental differences. First, for the the proposed color-gradient calculations with $w = 0.298$, the fingering transition occurs at $\mathrm{Ca} \approx 0.134$ whereas for standard color gradient, the fingering transition occurs at a lower capillary number of $\mathrm{Ca} \approx 0.127$. Also, after the transition to fingering—using the optimal w

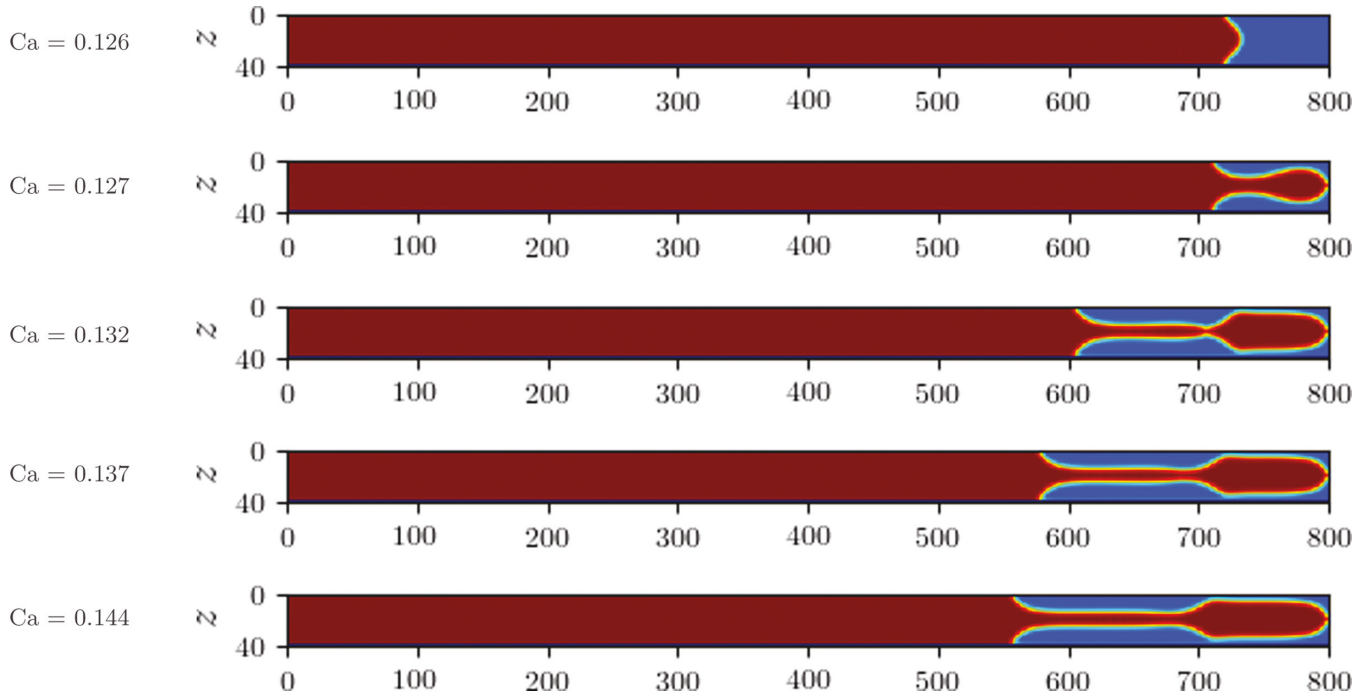

FIG. 15. Snapshots of flow in a pipe for wetting angle of $\theta = 0$ and various capillary numbers using the standard color-gradient calculations corresponding to a value of $w = 1$.

value—droplets occur at Ca ≈ 0.137, followed by a finger from Ca ≈ 0.140, droplets again at Ca ≈ 0.146, and finally a finger for Ca $\geqslant 0.154$. Note that we have performed simulations at Ca numbers ranging from Ca $= 0.130$ to 0.155 at intervals of ΔCa $= 0.001$ and the images in Fig. 14 and the capillary numbers in Table III summarize all of the transitions observed within this range of capillary numbers (i.e., no other transitions to droplets or fingering occurred other than the ones shown) when using the optimal value of $w = 0.298$ in the color-gradient calculations. In the case of the runs using the standard color-gradient calculation with $w = 1$, we observe only one transition to fingering behavior at Ca ≈ 0.127.

The lower capillary number predicted using the standard color-gradient calculation of the transition to fingering can be explained as follows. The fingering initiates at the front of the red fluid at 0°. Hence, the effective capillary number for fingering to initiate at 0° is $\mathrm{Ca}^* = \mu u_{\mathrm{in}}/\sigma^*_{0^\circ} = \mu u_{\mathrm{in}}/(g\sigma^*)$ where g is the factor decrease in interfacial tension lower along the Cartesian axes at 0°. So we have that the true capillary number of the transition to fingering is given by

$$\mathrm{Ca}^* \approx \frac{\mu u_{\mathrm{in}}}{\sigma_{0^\circ}} = \frac{\mu u_{\mathrm{in}}}{g\sigma^*} = \frac{1}{g}\frac{\mu u_{\mathrm{in}}}{\sigma^*} = \frac{1}{g}\mathrm{Ca}^*(w = 1). \tag{49}$$

From the previous section, we expect a decrease in interfacial tension of order 7% along the Cartesian axes for the standard color-gradient calculations with $w = 1$ and, hence, we can expect the value of $g \sim 0.93$ and, based on this, one may predict the true capillary number of the fingering transition from the apparent capillary number of the transition obtained using the standard color-gradient calculations as

$$\begin{aligned}\mathrm{Ca}^* &\approx \frac{1}{0.93}\mathrm{Ca}^*(w = 1) = \frac{0.127}{0.93} \\ &= 1.075 \times 0.127 \approx 0.1366,\end{aligned} \tag{50}$$

which is slightly higher than the capillary number of the fingering transition of $\mathrm{Ca}^*(0.298) = 0.134$ predicted using the proposed color-gradient calculation with $w = 0.298$. Namely, from the simulations we have

$$\begin{aligned}\mathrm{Ca}^*(w = 0.298) &= 0.134 \\ &= \frac{0.134}{0.127}\mathrm{Ca}^*(w = 1) \approx 1.055 \times 0.127.\end{aligned} \tag{51}$$

The proposed color-gradient calculations with the optimal w have the lowest anisotropy at the smallest radii of curvature so these should provide the most accurate estimate of the transition capillary numbers. The reason for the slight overprediction of $\mathrm{Ca}^* \approx 0.1366$ above which is higher than the value of $\mathrm{Ca}^*(0.298) = 0.134$ is likely the assumption of the 7% anisotropy whereas we should use the percentage

TABLE III. Table showing the key phenomena observed in simulation of flow in a pipe with the color gradient calculated using the optimal weight of $w = 0.298$.

Capillary number	Phenomenon	Transition
0.133	Meniscus	Pretransition to fingering
0.134	Fingering	First transition to fingering
0.137	Droplets	First transition to droplets
0.140	Fingering	Second transition to fingering
0.146	Droplets	Second transition to droplets
0.154	Fingering	Third transition to fingering

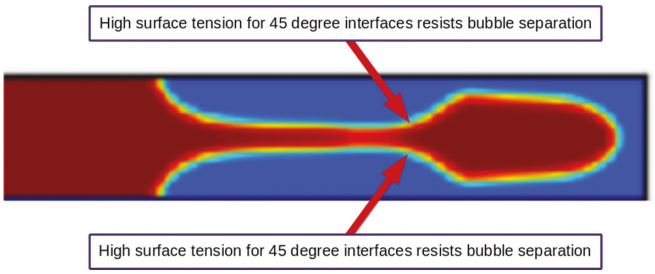

FIG. 16. Mechanism explaining how the anisotropy in the standard color-gradient calculation with $w = 1$ resists a finger head from breaking off and forming a droplet.

reduction in interfacial tension relative to the mean interfacial tension as measured during the Young-Laplace calculations of interfacial tension. An assumption of a 5% reduction in interfacial tension relative to the average would yield a precise prediction. However, there is no point to try to exactly predict this value as it is not clear what radius of curvature interface is the critical one for a finger to form (and, hence, exactly what percentage of anisotropy to use in this calculation). The analysis is intended only to demonstrate that the too low transition capillary number of the fingering predicted using the standard color-gradient calculation is expected because of the lower interfacial tension along Cartesian axes, and has a reasonable magnitude given the order of magnitude of the anisotropy. The proposed color-gradient calculations with $w = 0.298$ have the lowest anisotropy and, hence, provide the most accurate estimate of the capillary number transitions. In the above, we found that the size of the differences between the $w = 1$ capillary number transitions and the $w = 0.298$ transitions is adequately explained by the anisotropy of the $w = 1$ calculations.

The second and more fundamental difference between the simulation results of flow in a pipe using the standard and proposed color-gradient calculations is the existence of droplets at the transition to fingering using the proposed color-gradient calculations. This can be explained as follows. In these simulations, as the finger starts to form, a large head followed by a narrow tail appears (see $\mathrm{Ca} = 0.134$ of Fig. 14 and $\mathrm{Ca} = 0.127$ of Fig. 15). For the bulge at the head of the finger to break off and form a droplet, the interface at an angle of about 45° must be broken. However, for the standard color-gradient calculations, the color gradient and hence interfacial tension are larger at 45°. Hence, for the standard color-gradient calculation, this higher anisotropic interfacial tension at 45° resists formation of droplets. Figure 16 illustrates the proposed mechanism that explains why the standard color-gradient calculation for flow in a pipe failed to capture droplet formation whereas the proposed more isotropic color-gradient calculations did capture droplet formation.

We also did the same suite of runs using Leclaire's value of $w = 0.25$. Snapshots at the transition capillary numbers are shown in Fig. 17. Comparing to the results in Fig. 14, we see that using $w = 0.25$, one obtains the same fingering and droplet transitions, but they are shifted to slightly higher capillary numbers. Specifically, the first transition to fingering occurs at $\mathrm{Ca} \approx 0.135$ compared to $\mathrm{Ca} \approx 0.134$ for the runs using $w = 0.298$. Table IV compares the transition capillary

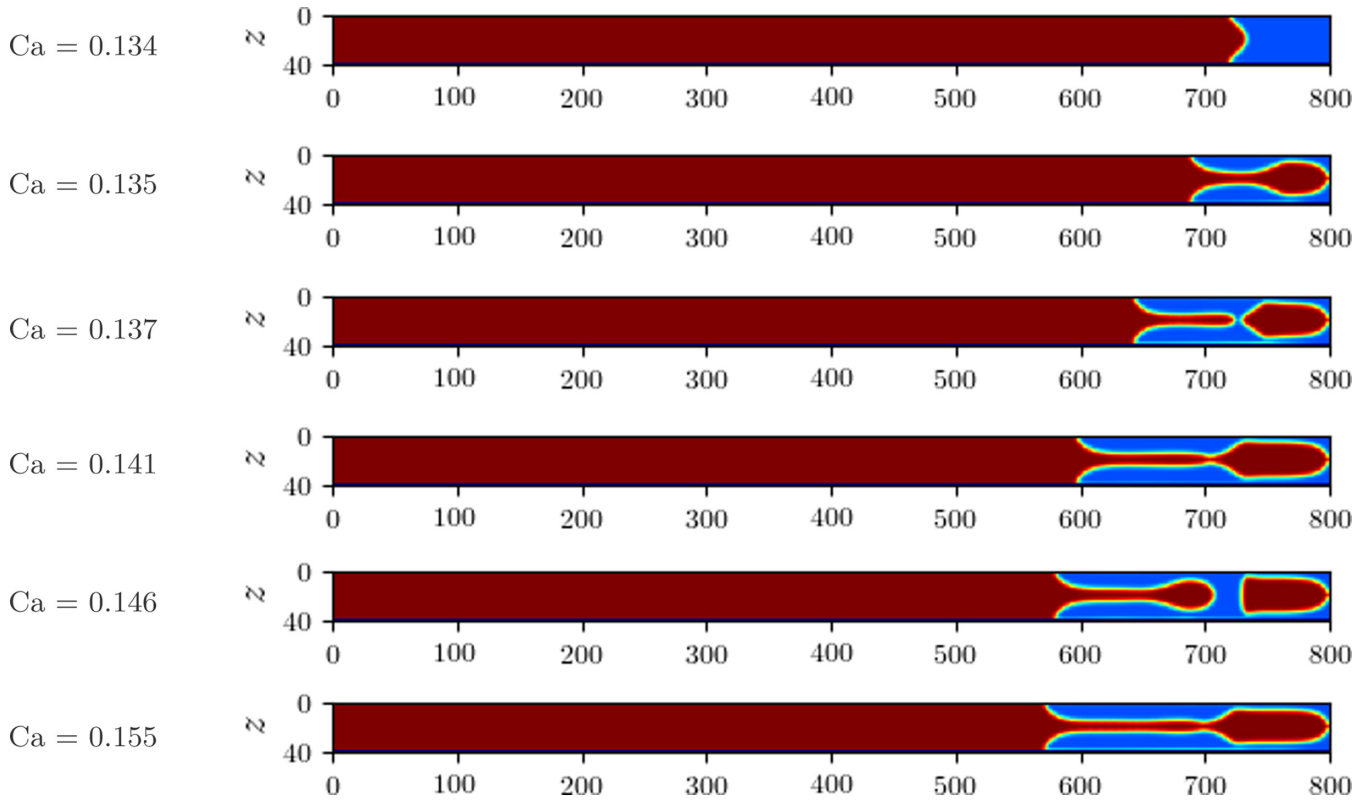

FIG. 17. Snapshots of flow in a pipe for wetting angle of $\theta = 0$ and various capillary numbers using Leclaire's value of $w = 0.25$ to calculate the color gradient.

TABLE IV. Table comparing the capillary numbers of transitions in simulation of flow in a pipe with the color gradient calculated using the optimal weight of $w = 0.298$ and Leclaire's value of 0.25.

Phenomenon	Transition	Ca ($w = 0.298$)	Ca ($w = 0.25$)
Meniscus	Pretransition to fingering	0.133	0.134
Fingering	First transition to fingering	0.134	0.135
Droplets	First transition to droplets	0.137	0.137
Fingering	Second transition to fingering	0.140	0.141
Droplets	Second transition to droplets	0.146	0.146
Fingering	Third transition to fingering	0.154	0.154

numbers for the two cases. Based on these results, there is a shift of order 0.005 to higher capillary numbers in the $w = 0.25$ runs. This can again be explained by the slight anisotropy of the $w = 0.25$ run. From Fig. 12, we know that using $w = 0.25$ leads to a -1.4% anisotropy, which means that the color gradient is about 1.4% higher along the Cartesian axes. Hence, as was done in the analysis above, we can estimate the true capillary number of the first fingering transition as

$$\mathrm{Ca}^* \approx \frac{1}{1.014}\mathrm{Ca}^*(w = 0.25) = \frac{0.135}{1.14} = 0.986 \times 0.135 \approx 0.133. \tag{52}$$

As explained above, this is an overestimate of the correction since one should use the percent anisotropy relative to an average but, again, this level of detail in the analysis is not warranted given that the anisotropy at the critical radius of curvature at which a pinchout occurs is not exactly known. The only purpose of the above analysis is to demonstrate that due to the slight anisotropy using $w = 0.25$, the capillary number of fingering transitions is slightly overpredicted, which explains the slightly higher transition capillary numbers of the $w = 0.25$ runs compared to the $w = 0.298$ runs. Based on the above analyses, and given that the $w = 0.298$ weight minimizes color-gradient anisotropy to less than 0.66% with a mean anisotropy of 0.12% for small radius of curvature interfaces, we propose that the proposed weight for diagonal nearest neighbors is optimal for correctly capturing pore scale phenomena such as fingering and droplet formation, and that this weight will lead to the most accurate quantification of transition capillary numbers.

VII. NONPHYSICAL PRESSURE GRADIENTS AND SPURIOUS CURRENTS

Another advantage of the proposed color-gradient calculations is that it significantly attenuates nonphysical static droplet pressure gradients that exist using the standard color-gradient calculations due to the relatively high surface-tension anisotropy, and which lead to significant spurious currents. Preliminary studies suggest that the level of attenuation is roughly an order of magnitude, similar to that reported by Leclaire *et al.* [21] using $w = 0.25$. Using the proposed optimal w value or Leclaire *et al.*'s value of $w = 0.25$ leads to a much more homogeneous pressure field inside and around the edges of a static droplet, even to very low interfacial tensions of $\sigma \sim 5 \times 10^{-12}$ which is down to the limit of numerical precision. This improved accuracy gives confidence that, as is the case using Leclaire *et al.*'s color-gradient calculations with $w = 0.25$, the proposed color-gradient calculations will enable a large range of interfacial tensions to be more accurately simulated. To illustrate the attenuation of spurious currents down to $A = 10^{-11} \Rightarrow \sigma \sim 5 \times 10^{-12}$, we defined a static droplet with $r_0 = 8$ and calculated the maximum magnitude of the spurious currents for the cases of $w = 1$ (standard case), $w = 0.25$ (Leclaire's value), and $w = 0.298$ (optimal w for the $r_0 = 2$ case) at various A. Table V shows these results and demonstrates that the spurious currents at the optimal w are about ten times smaller than those in the standard case ($w = 1$), and about two times smaller than Leclaire's case ($w = 0.25$).

VIII. CONCLUSIONS

The Rothman-Keller color-gradient lattice Boltzmann method is a powerful method to simulate multiphase flow. At its heart is a calculation of the gradient $\mathbf{F}$ of the color difference $D = (\rho_r - \rho_b)$ between two fluids. It is well known that the surface tension using the standard color-gradient calculation is anisotropic, leading to nonphysical spurious currents, and potentially an inability to correctly model certain pore scale phenomena. The standard second order accurate color-gradient calculation is one option to calculate the gradient. Improved accuracy can be achieved by using higher order finite-difference calculations but these are computationally expensive and, also, the calculations near walls remain only second or first order accurate. Alternatively, a better choice of the relative weights of the nearest neighbors when calculating the second order accurate color gradients leads to improved isotropy. One such choice is a relative weight of $w = 0.25$ for diagonal nearest neighbors as developed by Leclaire *et al.* [21] based on achieving isotropy of the error in the gradient to second order. In contrast, we have investigated the anisotropy of the color gradient of droplets of varying sizes over the full range of diagonal weights w and for several typical interface smoothing parameters β to study whether there may be an even more optimal choice. We first present the general formula for second order accurate finite-difference calculations of the color gradient which allows the weight w of nearest neighbors along diagonals to be varied relative to those along the Cartesian axes. We have then studied the anisotropy of the color gradient for varying weights w for small radius of curvature droplets. We have found that for interface smoothing parameters of $\beta = (0.5, 0.7, 0.99)$, the use of weights of $w = (0.298, 0.284, 0.275)$ for diagonal nearest neighbors in the color-gradient calculations minimizes the

TABLE V. Magnitude of spurious currents scaled by the interfacial tension parameter, i.e., $\max(|\mathbf{u}|/A)$ as a function of A for the cases of $w = 1$, 0.25, and 0.298 for a static droplet with $r_0 = 8$.

			$\max(\lvert\mathbf{u}\rvert/A)$		
w	$A = 0.1$	$A = 0.01$	$A = 0.001$	$A = 10^{-11}$	$A = 10^{-12}$
1	0.00898	0.0116	0.0215	0.0249	0.0252
0.25	0.00110	0.00206	0.00467	0.00559	0.00808
0.298	0.00128	0.00146	0.00211	0.00254	0.00935

anisotropy to a fraction of a percent for the smallest droplets to (0.66%,0.35%,0.67%) and minimizes the mean anisotropy to (0.12%,0.02%,0.085%). In contrast, the standard color-gradient calculation which weights the diagonal nearest neighbors equally (i.e., $w = 1$) has much higher anisotropy and mean anisotropy, respectively, of (7.1%,6.4%,5.9%) and (4.2%,3.8%,2.8%). And use of Leclaire's value of $w = 0.25$ has anisotropy of (1.4%,.62%,1.15%) and mean anisotropy of (0.4%,0.32%,0.09%). Hence, our proposed optimal w values yield much greater isotropy than the standard $w = 1$ value, and significantly greater isotropy than Leclaire's value. We present an example that shows that the anisotropy of the standard color-gradient calculations can lead to fundamentally different behavior at critical capillary numbers such as at the transition to fingering.

In this example, we inject a nonwetting red fluid into a pipe filled with a blue fluid of the same viscosity, and we observe droplet formation at the transition capillary number to fingering using the proposed color-gradient calculations with $\beta = 0.5$ and $w = 0.298$, whereas using the standard $w = 1$ color-gradient calculations, no such droplets are observed. We present an explanation for why the droplet formation is inhibited by the anisotropic surface tension of the standard color-gradient calculations. Leclaire's value of $w = 0.25$ also predicts the droplet formation. However, there may be other cases where the factor of 2 lower anisotropic error and up to 15 times lower mean anisotropic error for $\beta = 0.7$ using our proposed optimal w values compared to using Leclaire's $w = 0.25$ value is significant. As such, we recommend for the cases of $\beta = (0.5, 0.7, 0.99)$ the use of $w = (0.298, 0.284, 0.275)$ when using second order accurate RK color-gradient calculations. These w values represent an optimal choice to minimize surface-tension anisotropy of small radius of curvature interfaces and, hence, to most accurately model and study pore scale processes, a major target of the RK LBM, where surface-tension isotropy of narrow fingers and small droplets plays a crucial role in correctly capturing phenomenology.

We note that as was the case for Leclaire's improved value of $w = 0.25$, the use of the proposed optimal w values also decreases nonphysical heterogeneous pressure fields and spurious currents around the edges of static droplets which result from surface-tension anisotropy, and increases the range of interfacial tensions that can be accurately modeled. Namely, the spurious currents are around an order of magnitude lower using the optimal value of $w = 0.298$ compared to using the standard value of $w = 1$, and about twice lower than using Leclaire's value of $w = 0.25$ over a range of ten orders of magnitude of the surface-tension parameter A.

In conclusion, the RK LBM is a powerful method to study multiphase flow at the pore scale but requires sufficiently isotropic calculations of the color gradient to reliably predict phenomena. Such isotropy cannot be achieved using the widely applied standard second order accurate finite-difference scheme using $w = 1$. Vastly improved isotropy can be achieved with Leclaire's weight of $w = 0.25$ for diagonal nearest neighbors, and so at a minimum, this value should be applied rather than the standard color-gradient calculations. We show that an even greater isotropy can be achieved for small radius of curvature interfaces using values of $w = (0.298, 0.284, 0.275)$ for the cases of $\beta = 0.5, 0.7, 0.99)$, and as such, we propose these values as the optimal weights for RK color-gradient LBM simulations and related variants that aim to study pore scale phenomena such as fingering and droplet formation. There remains no justification for any researcher to continue to use the standard color-gradient calculation. Either our proposed optimal weights or, at the very least, Leclaire *et al.*'s value of $w = 0.25$ should be used to weight the diagonal nearest neighbors in the CG calculation. The computational cost is identical and the surface-tension isotropy is dramatically improved.

ACKNOWLEDGMENTS

D.A.Y. would like to thank the National Science Foundation's Geochemistry and CISE program for support. In addition, this research was in part funded by U.S. Department of Energy Grant No. DE-SC0019759 (D.A.Y.) and by National Science Foundation Grant No. EAR-1918126 (D.A.Y.).

[1] U. Frisch, B. Hasslacher, and Y. Pomeau, Lattice-Gas Automata for the Navier-Stokes Equation, Phys. Rev. Lett. **56**, 1505 (1986).

[2] P. L. Bhatnagar, E. P. Gross, and M. Krook, A model for collision processes in gases. I. Small amplitude processes in charged and neutral one-component systems, Phys. Rev. **94**, 511 (1954).

[3] Y.-H. Qian, D. d'Humières, and P. Lallemand, Lattice BGK models for Navier-Stokes equation, Europhys. Lett. **17**, 479 (1992).

[4] S. Chen and G. D. Doolen, Lattice Boltzmann method for fluid flows, Annu. Rev. Fluid Mech. **30**, 329 (1998).

[5] H. Huang, M. Sukop, and X. Lu, *Multiphase Lattice Boltzmann Methods: Theory and Application* (Wiley, New York, 2015).

[6] S. Succi, *The Lattice Boltzmann Equation: For Fluid Dynamics and Beyond* (Oxford University, New York, 2001).

[7] S. Succi and S. Succi, *The Lattice Boltzmann Equation: For Complex States of Flowing Matter* (Oxford University, New York, 2018).

[8] T. Krüger, H. Kusumaatmaja, A. Kuzmin, O. Shardt, G. Silva, and E. Viggen, *The Lattice Boltzmann Method: Principles and Practice* (Springer, New York, 2017), p. 482.

[9] X. He, S. Chen, and R. Zhang, A lattice Boltzmann scheme for incompressible multiphase flow and its application in simulation of Rayleigh-Taylor instability, J. Comput. Phys. **152**, 642 (1999).

[10] Z. Guo, B. Shi, and C. Zheng, A coupled lattice BGK model for the Boussinesq equations, Int. J. Numer. Methods Fluids **39**, 325 (2002).

[11] X. Shan, Simulation of Rayleigh-Bénard convection using a lattice Boltzmann method, Phys. Rev. E **55**, 2780 (1997).

[12] J. Wang, D. Wang, P. Lallemand, and L.-S. Luo, Lattice Boltzmann simulations of thermal convective flows in two dimensions, Comput. Math. Appl. **65**, 262 (2013).

[13] S. Arun, A. Satheesh, C. Mohan, P. Padmanathan, and D. Santhoshkumar, A review on natural convection heat transfer problems by lattice Boltzmann method, J. Chem. Pharm. Sci **10**, 635 (2017).

[14] P. Mora and D. A. Yuen, Simulation of plume dynamics by the lattice Boltzmann method, Geophys. J. Int. **210**, 1932 (2017).

[15] P. Mora and D. A. Yuen, Simulation of regimes of convection and plume dynamics by the thermal lattice Boltzmann method, Phys. Earth Planet. Inter. **275**, 69 (2018).

[16] X. Shan and H. Chen, Lattice Boltzmann model for simulating flows with multiple phases and components, Phys. Rev. E **47**, 1815 (1993).

[17] M. Latva-Kokko and D. H. Rothman, Static contact angle in lattice Boltzmann models of immiscible fluids, Phys. Rev. E **72**, 046701 (2005).

[18] M. R. Swift, E. Orlandini, W. R. Osborn, and J. M. Yeomans, Lattice Boltzmann simulations of liquid-gas and binary fluid systems, Phys. Rev. E **54**, 5041 (1996).

[19] T. Inamuro, T. Ogata, S. Tajima, and N. Konishi, A lattice Boltzmann method for incompressible two-phase flows with large density differences, J. Comput. Phys. **198**, 628 (2004).

[20] P. Lallemand and L.-S. Luo, Theory of the lattice Boltzmann method: Dispersion, dissipation, isotropy, galilean invariance, and stability, Phys. Rev. E **61**, 6546 (2000).

[21] S. Leclaire, M. Reggio, and J.-Y. Trépanier, Isotropic color gradient for simulating very high-density ratios with a two-phase flow lattice Boltzmann model, Comput. Fluids **48**, 98 (2011).

[22] H. Huang, J.-J. Huang, and X.-Y. Lu, Study of immiscible displacements in porous media using a color-gradient-based multiphase lattice Boltzmann method, Comput. Fluids **93**, 164 (2014).

[23] S. Leclaire, A. Parmigiani, O. Malaspinas, B. Chopard, and J. Latt, Generalized three-dimensional lattice Boltzmann color-gradient method for immiscible two-phase pore-scale imbibition and drainage in porous media, Phys. Rev. E **95**, 033306 (2017).

[24] S. Leclaire, M. El-Hachem, J.-Y. Trépanier, and M. Reggio, High order spatial generalization of 2d and 3d isotropic discrete gradient operators with fast evaluation on gpus, J. Sci. Comput. **59**, 545 (2014).

[25] B. Fornberg, Generation of finite difference formulas on arbitrarily spaced grids, Math. Comput. **51**, 699 (1988).

[26] D. H. Rothman and J. M. Keller, Immiscible cellular-automaton fluids, J. Stat. Phys. **52**, 1119 (1988).

[27] A. K. Gunstensen, D. H. Rothman, S. Zaleski, and G. Zanetti, Lattice Boltzmann model of immiscible fluids, Phys. Rev. A **43**, 4320 (1991).

[28] D. Grunau, S. Chen, and K. Eggert, A lattice Boltzmann model for multiphase fluid flows, Phys. Fluids A **5**, 2557 (1993).

[29] T. Reis and T. N. Phillips, Lattice Boltzmann model for simulating immiscible two-phase flows, J. Phys. A **40**, 4033 (2007).

[30] Q. Zou and X. He, On pressure and velocity flow boundary conditions and bounce back for the lattice Boltzmann BGK model, Phys. Fluids **9**, 1591 (1997).